

Coda wave seismic structure beneath the Indian Ocean region and its implications to seismotectonics and structural heterogeneity



Mamuni Sacheeta Ekka^a, Vandana^b, P.N.S. Roy^{a,c,*}, O.P. Mishra^b

^a Department of Applied Geophysics, Indian Institute of Technology (Indian School of Mines), Dhanbad 826004, Jharkhand, India

^b National Centre for Seismology (NCS), ESSO – Ministry of Earth Sciences (MoES), Lodi Road, New Delhi, India

^c Department of Geology and Geophysics, Indian Institute of Technology, Kharagpur 721302, West Bengal, India

ARTICLE INFO

Keywords:

Seismic Coda waves
Attenuation structure
The Indian Ocean region
Structural heterogeneity
Seismogenesis
Earthquake hazards

ABSTRACT

The Indian Ocean region is one of the challenging areas for seismological research because of its complex seismotectonic settings and intricate structural heterogeneity prevails beneath the Indian Ocean region. In order to address the problem we attempted to determine the attenuation structure for the Indian Ocean region using coda wave generation by single backscattering model. In this study, the central frequency of interest has been considered between 1.5 and 12.0 Hz with lapse time window (LTW) of 20, 30, 40, 50 and 60 s measured from the origin time of the earthquake. We obtained the attenuation relation for different seismotectonic zones associated with varying estimate of attenuation parameters; Spreading Zone [$Q_{c(SPZ)} = 171f^{1.10}$]; Subduction Zone [$Q_{c(SZ)} = 220f^{0.961}$]; Triple Point Junction [$Q_{c(TPJ)} = 156f^{1.15}$]; Prominent faults of Indian Ocean region [$Q_{c(PFOZ)} = 197f^{0.99}$] and Volcanic and Hotspot [$Q_{c(VZ, HS)} = 209f^{0.97}$]. We estimated average frequency-dependent attenuation parameters of Q_0 that varies as $156 \pm 32 \leq Q_0 \leq 220 \pm 33$ with corresponding variability in frequency parameter (θ) as $0.96 \pm 0.05 \leq \theta \leq 1.15 \pm 0.09$ at 40 s LTW for the entire Indian Ocean region, suggesting that the entire Indian Ocean is seismo-tectonically highly active and is attributed to the nature and extent of attenuation due to varying amount of structural heterogeneity in different tectonic zones characterized by the occurrence of earthquakes of varying strengths in the seismically active tectonic zones of the region. We found that the triple Junction (RTJ) is associated with low- Q_c and high attenuation because of deposition of a variety of sediments at the RTJ, which is in unison to the geological mapping of the region. We observed that our estimated attenuation model is comparable that of the Aleutian Islands (the Adak Seismic zone) at low frequency (≤ 5 Hz) and to the Philippine Sea Subduction zone (Petukhin) at higher frequency range (≥ 5 Hz), which is very much correlative to seismo-tectonic settings. We infer that our assimilated attenuation model has potential to provide information on intricate seismotectonics and seismogenesis for computing earthquake source parameters, and earthquake hazards that may be useful for assimilating detailed seismic velocity structure beneath the Indian Ocean region.

1. Introduction

The characteristics of seismic wave attenuation are very important for determining the physical state and condition of the earth's interior (Aki, 1980). Usually, these are dependent on crustal properties of the region related to density and composition of the earth crust, degree of heterogeneity, amount of asperities and irregularities in formation histories of sub-surface rock materials (Mishra et al., 2005a,b). It is useful for the study of the source mechanism, evaluation of seismic hazard assessment and risk analysis and understanding the regional geodynamic processes involved in earthquake genesis beneath the seismically active region. It is observed that seismic wave attenuation

are dictated by numerous factors, such as, geometrical spreading in which wave-front emanating from point source spread all over the spherical surface with increasing size; intrinsic attenuation, which is partly due to absorption of energy by imperfect elastic properties and partly due to the exchange of potential energy and kinetic energy by heating up of the medium; scattering attenuation associated with heterogeneous medium that lead to a decrease in amplitude with travel time-distance (Aki, 1980). Seismic wave attenuation property of a medium is measured by a dimensionless quantity referred to as quality factor $Q = 2\pi E/\Delta E$, which is defined as the ratio of total stored energy to the energy loss per oscillation cycle (Knopoff, 1964; Jackson and Anderson, 1970; Aki and Chouet, 1975), where E is the total amount of

* Corresponding author.

E-mail addresses: pns_may1@yahoo.com (P.N.S. Roy), omp.mishra@nic.in, opmishra2010.saarc@gmail.com (O.P. Mishra).

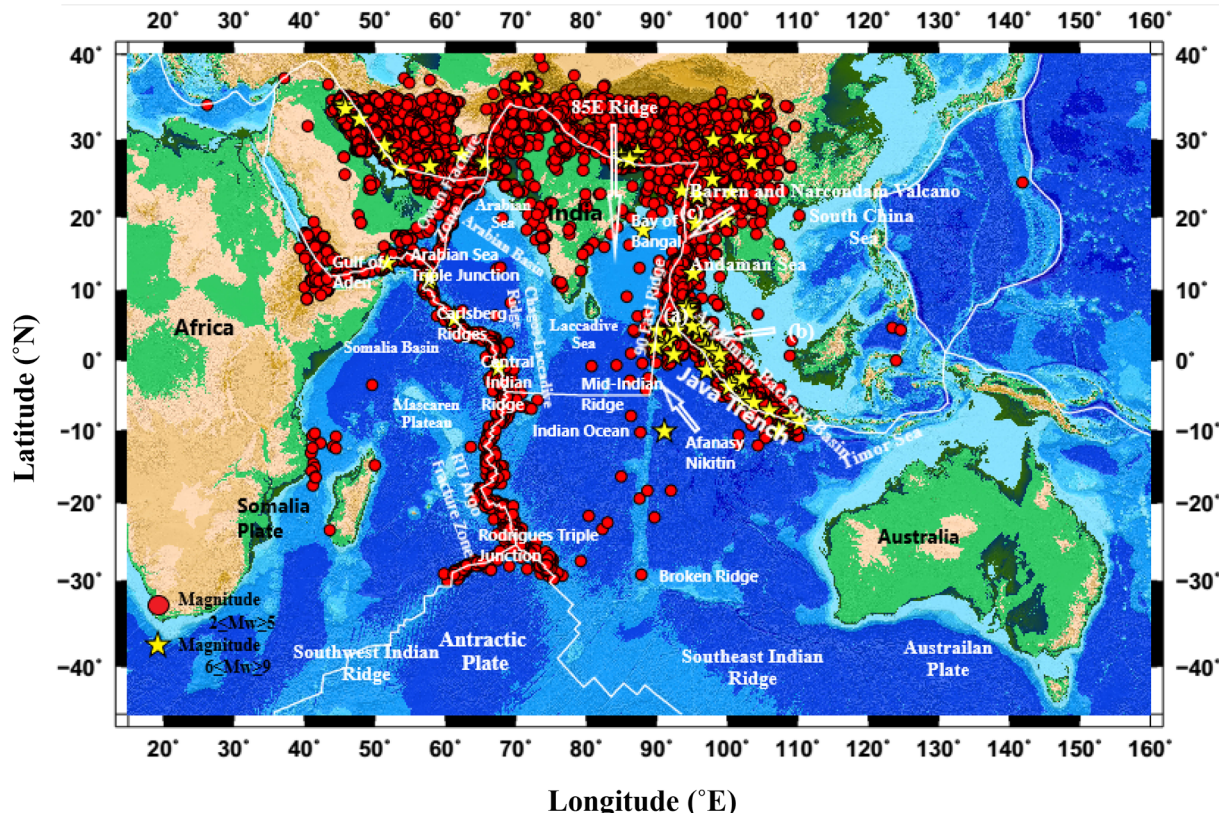


Fig. 1. Plate tectonic map of the study region with seismicity recorded in the Indian Ocean from 2013 to 2018 and reported by IRIS Network. The West Andaman Fault (a), The Sumatran fault (b), The Sagging Fault across the Andaman-Nicobar ridge (c). The red circle marked by magnitude $2 \leq Mw \geq 5$ and black star marked by magnitude $6 \leq Mw \geq 9$. (For interpretation of the references to colour in this figure legend, the reader is referred to the web version of this article.)

energy per cycle and ΔE is the part of total energy E dissipated per cycle. The characteristics of coda wave, “ Q_c ”, are described as the end portion of a seismogram when all the seismic wave phases get arrived (Aki, 1969). The wave-front envelope of the tail portion of seismogram is known as coda that arrives on different time intervals at the station. Usually, the nature of decay for these waves in a seismogram with time, ensemble the average attenuation properties of the material instead of the feature of a single trajectory from source to receiver (Gupta et al., 1998; Paul et al., 2003; Mishra et al., 2005a,b).

In order to reveal the crust and upper mantle heterogeneities, the coda wave attenuation by the single backscattering method given by Aki and Chouet (1975) has been used to estimate the frequency-dependent attenuation relationships for this region. The superposition of backscattered coda waves is randomly distributed by numerous heterogeneities present in the earth's crust and upper mantle (Aki, 1969; Aki and Chouet, 1975; Rautian and Khalturin, 1978). Such scatterings are produced due to irregular and complex surface topography, faults, fractures, and the heterogeneity in the elastic rocks. Coda Q helps to understand the tectonic activities, where stable region is characterized by high-Q value and seismically active region characterized by low-Q value (Pujades et al., 1990; Herrmann, 1980). Diverse tectonic regions of different parts of the world revealed different average attenuation relationship, such as, South India, $Q = 460f^{0.83}$ (Rao et al., 1998); New England, $Q = 460f^{0.40}$ (Pulli, 1984); Eastern North America, $Q = 680f^{0.36}$ (Atkinson and Boore, 1995); North Iberia $Q = 600f^{0.45}$ (Pujades et al., 1997); Indian Shield, $Q = 800f^{0.42}$ (Singh et al., 2004); NE U.S., $Q = 900f^{0.35}$ (Singh and Herrmann, 1983); Central U.S., $Q = 1000f^{0.20}$ (Singh and Herrmann, 1983); Canadian Shield, $Q = 900f^{0.20}$ (Hasegawa, 1985) and Central Mississippi Valley (CENA), $Q = 210f^{0.78}$ (Dwyer et al., 1984); Aleutian Islands, $Q = 214f^{1.05}$ (Scherbaum and Kisslinger, 1985); Koyna, India, $Q = 96f^{1.09}$ (Gupta

et al., 1998); Bhuj, India, $Q = 102f^{0.98}$ (Mandal et al., 2004); Western U.S., $Q = 150f^{0.40}$ (Singh and Herrmann, 1983); and for NW Himalaya, $Q = 126f^{1.12}$ (Vandana et al., submitted for publication). Moreover, the seismic coda wave attenuation provided significant information and a great help in understanding of many geophysical mechanisms related to intrusion and associative processes with rock materials (e.g., Guo et al., 2009). Several studies have been carried out to investigate the kinematics of attenuation properties for different regions of the world to understand the diverse characteristics of attenuation behaviors of the media in which seismic wave travels (e.g., Campillo et al., 1985; Kvamme and Havskov, 1989; Yoshimoto et al., 1993; Aki, 1996; Mak et al., 2004; Singh et al., 2004; Kumar et al., 2005, 2014, 2015, 2016; Biescas et al., 2007; Mohamed et al., 2010; Mukhopadhyay and Sharma, 2010; Dobrynina, 2011; Padhy et al. 2011; Gupta et al., 2012; Akyol, 2015; Vandana et al., 2016; Naghavi et al., 2017; Das et al., 2018; Singh et al., 2018; Kumar and Yadav, 2019).

The Indian Ocean province is regarded as a unique and the most seismotectonically active by its complex geological setting structure region, where several geophysical studies have been attempted (Fig. 1). In this study, we estimated the coda wave attenuation property to reveal the physical state at different parts to map the subsurface tectonics structure of region by studying regional variation which may provide valuable evidence for understanding the seismic structure of the Indian Ocean region and its seismogenic potential associated with the structural heterogeneity. Our study evaluates the spatial distribution of coda wave attenuation using the best located 300-earthquakes ($Mw \geq 5$) (Table 1) beneath the Indian Ocean, which provides possible reason of varying distribution of attenuation characteristics in and around historically large to great earthquakes occurred in the region (Table 2). The study region has been demarcated into a total of five tectonic blocks (Table 3) having bearing on earthquake hazards in the coastal

Table 1

Hypocentral parameters of 300-earthquakes used in this study after their relocations, where; ERX: error in longitude; ERY: error in latitude; ERZ: error in depth; N: Number of station recorded the earthquake.

S.No.	Date	Time	Longitude	Latitude	Depth (km)	Magnitude M _w	RMS (s)	ERX (km)	ERY (km)	ERZ (km)	N
1	01-01-14	0:01:21	120.22	19.1	34.1	5	0.03	0.9	1	3.8	6
2	02-01-14	19:30:56	120.24	19.19	28.2	5	0.03	1.4	2.6	9.1	6
3	23-01-14	0:52:16	120.29	-7.13	590	5.3	0.03	1	1.4	3.6	7
4	25-01-14	5:14:21	109.22	-8.04	87.8	6.2	0.06	1.3	1	3.3	5
5	26-01-14	12:38:40	95.8	22.93	32	5.4	0.02	1.5	6.5	6.4	5
6	26-01-14	17:57:46	121.93	13.49	30.2	5.1	0.03	1.4	1.7	7	5
7	27-01-14	16:14:00	109.25	-8.15	83	5	0.01	1.5	2.3	14	5
8	01-02-14	20:13:33	68.58	-5.12	13	5.2	0.38	1.9	1.9	2.3	6
9	02-02-14	18:51:11	120.29	20.2	18.5	5.1	0.32	4.9	3.6	3.5	3
10	10-02-14	18:06:20	124.58	-8.23	33.1	5.5	0.34	7.4	6.4	10.8	4
11	13-02-14	18:57:38	58.17	9.26	21	5.4	0.23	4.9	2.7	3.9	3
12	17-02-14	5:56:01	120.46	18.48	28.6	5.5	0.03	5.6	1.4	3.2	6
13	18-02-14	3:34:13	122.94	1.67	45.5	5.3	0.01	4.7	3.4	17.1	3
14	22-02-14	17:29:51	97.28	1.18	28.8	5.3	0.46	1.2	2.3	5.7	12
15	23-02-14	21:21:17	117.94	-9.91	45.3	5	0.02	1.3	1.3	8.2	6
16	24-02-14	23:32:48	62.71	4.1	12.7	5.6	0.43	2.9	2.5	1.2	3
17	25-02-14	2:01:26	62.52	4.31	19.4	5.4	0.91	3.4	3.9	3.5	10
18	28-02-14	2:28:38	120.31	20.21	16.3	5.1	0.8	1.8	3.9	3.1	4
19	28-02-14	5:50:37	94.23	7.27	88.9	5.2	0.2	2.2	2.8	1.8	4
20	06-03-14	10:24:00	117.07	-7.69	299	5.1	0.2	3.3	2.9	2	3
21	07-03-14	16:14:54	103.76	-4.54	119.2	5.3	0.02	3.8	5	1.5	3
22	09-03-14	13:42:20	113.01	-8.98	85.7	5.2	0.5	3.8	3	2	3
23	14-03-14	13:38:09	94.23	7.69	29.7	5.4	0.44	4.2	5.7	2.9	10
24	15-03-14	2:59:31	57.17	13.84	21	5	0.32	3.4	3.6	2.5	4
25	15-03-14	10:58:46	99.02	2.81	171.4	5.4	0.03	3.9	2.3	7.9	4
26	19-03-14	20:51:34	108.28	-8.6	90.1	5.5	0.61	1.9	1.3	1.2	3
27	20-03-14	21:33:02	114.22	-9.63	65.6	5.1	0.25	1.8	2.4	1.4	3
28	21-03-14	13:41:10	94.23	7.68	19.3	6.4	0.03	0.2	0.3	0.5	13
29	21-03-14	14:11:15	94.26	7.56	17.7	5.6	0	1.2	3.9	1.5	3
30	21-03-14	14:25:10	94.21	7.46	16.6	5.5	0.01	1.4	1.6	2.5	4
31	21-03-14	21:03:43	94.2	7.41	17	5.2	0.44	3	5.2	1.1	10
32	27-03-14	4:00:18	86.69	4.32	28.6	5.3	0.01	1.4	2.2	3.2	4
33	03-04-14	9:30:23	102.17	-5.32	29	5.5	0.03	0.2	0.4	0.7	10
34	17-04-14	4:38:18	122.99	4.51	578.9	5.8	0.01	2.1	1.3	3.8	3
35	17-04-14	13:03:04	117.48	-7.85	282.2	5.4	0.02	1.5	1.2	5.4	3
36	18-04-14	13:33:38	110.44	-9.08	31.4	5.2	0.02	1.1	0.8	2.1	5
37	20-04-14	8:43:51	98.32	0.57	37.3	5.2	0.5	1.5	2.2	1.9	4
38	21-04-14	20:45:24	120.03	17.35	30.2	5.4	0.59	6.3	4.9	14.8	7
39	28-04-14	0:43:53	120.09	19.68	18.7	5.4	0.02	1.8	1	4.3	3
40	01-05-14	14:35:39	97.95	1.97	50.3	5.8	0.49	3.1	4.4	4	8
41	03-05-14	14:47:07	97.9	1.96	60.1	5.3	0.5	1	1.7	1.1	8
42	05-05-14	11:08:46	99.7	19.62	15.2	6.1	0.47	3.3	5	4.4	10
43	06-05-14	0:50:17	99.63	19.6	14.7	5.2	0.33	2.7	4.9	4.6	5
44	06-05-14	0:58:21	99.44	19.61	10.1	5.3	0.18	4.9	4.8	4.1	5
45	10-05-14	2:42:12	117.53	-8.17	232.8	5.5	0.14	2.5	2.8	1.9	4
46	12-05-14	3:36:04	68.54	-4.86	13	5.2	0.49	1.7	1.9	1.7	7
47	15-05-14	10:16:44	122.04	9.35	30.1	6.1	0.02	1.2	0.8	2.9	5
48	18-05-14	1:02:32	92.74	4.24	32.9	6	0.59	1.3	2.2	5.2	12
49	18-05-14	10:59:24	93.85	3.17	18	5.5	0.49	1.6	3.3	2.4	8
50	21-05-14	16:21:54	88.06	18.24	45.1	6	0.34	1	3.7	2.1	11
51	23-05-14	9:06:56	102.63	-6.98	16.8	5.1	0.47	5.1	4.8	4.1	11
52	27-05-14	4:25:20	67.06	-15.16	16	5.3	0.57	1.5	2.4	4.8	13
53	30-05-14	0:56:20	119.59	-8.4	180.2	5.1	0.14	4.2	3.3	4.5	3
54	01-06-14	10:07:13	89.77	1.98	23.6	5.8	0.27	2	3.8	3.4	13
55	09-06-14	21:45:15	122.16	10.04	22.3	5.3	0.51	2.9	2.8	2.1	3
56	14-06-14	11:11:03	91.04	-10.11	23.1	6.5	0.03	0.2	0.3	0.2	15
57	19-06-14	0:51:18	102.37	-2.78	170.9	5	0.02	1.8	4.1	9.1	3
58	21-06-14	21:51:52	122.95	-0.07	125.9	5.4	0.02	4.4	4.6	3.9	4
59	22-06-14	6:38:51	108.02	-7.79	76.9	5.1	0.02	2.6	2.7	2.2	3
60	25-06-14	11:52:03	120.58	13.57	71.3	5.5	0.06	1.4	2	1.2	4
61	26-06-14	0:12:26	118.26	-9.65	100	5	0.48	1.9	1.5	0.8	3
62	26-06-14	11:28:23	123.39	-0.01	155.6	5.2	0.01	2.2	2.1	6.8	5
63	02-07-14	7:24:29	124.65	0	71.4	5.2	0.1	3.4	3.9	2.8	9
64	05-07-14	9:39:28	96.94	1.93	20	6	0.41	1.9	1.5	1.4	11
65	07-07-14	9:15:28	123.72	-7.29	547	5.4	0.01	1.6	2.1	1.1	3
66	14-07-14	5:05:03	111.25	-8.82	52.5	5.4	0.01	3.4	1.8	10.1	4
67	17-07-14	6:11:51	121.47	22.14	10	5	0.42	2.8	4.5	4.1	13
68	19-07-14	14:14:02	57.96	11.71	10	6.3	0.19	1.9	3.7	9.1	12
69	24-07-14	8:41:08	111.58	-9.13	35	5.4	0.22	1.2	2.6	1.1	6
70	28-07-14	8:03:08	66.85	-17.23	0	5.5	0.18	3.5	4.8	3.3	4
71	29-07-14	7:07:07	93.09	14.36	12	5.4	0.91	4.4	4.9	3.1	11
72	29-07-14	7:16:41	87.7	-10.21	10	5.1	0.08	1	1.4	1.1	12

(continued on next page)

Table 1 (continued)

S.No.	Date	Time	Longitude	Latitude	Depth (km)	Magnitude M _w	RMS (s)	ERX (km)	ERY (km)	ERZ (km)	N
73	31-07-14	13:41:00	95.19	12.39	12	5.8	0.37	2.7	2.1	1.6	11
74	02-08-14	10:33:24	67.3	-9.08	10	5.6	0.3	2.6	3.9	1.5	9
75	04-08-14	10:36:10	94.65	5.4	57	5	0.21	1.5	4.1	3.3	3
76	08-08-14	16:57:01	99.07	2.43	151.7	5.9	0.31	1.2	1.1	0.9	3
77	17-08-14	16:04:49	68.43	-20.78	10	5.1	0.45	2.6	2.7	2.5	10
78	03-09-14	13:43:58	122.43	15.17	10	5.1	0.4	1.6	1.7	1.2	3
79	09-09-14	9:28:22	93.24	22.2	10	5.4	0.02	0.8	1.5	2.4	11
80	11-09-14	4:32:43	90.38	2.61	15.4	5	0.02	1.1	1.6	8.3	7
81	14-09-14	4:52:27	97.26	1.15	36.6	5.5	0.57	4.9	3.8	1.5	12
82	14-09-14	16:34:23	97.24	1.13	38.6	5.1	0.3	3.6	3.9	2.8	5
83	20-09-14	4:26:12	125.23	6.86	25.7	5.2	0.01	1.6	2.7	3.8	5
84	23-09-14	10:22:20	119.98	0.11	69.2	5.3	0.01	1.7	1.5	1.4	3
85	25-09-14	8:29:58	95.56	6	194.7	5.2	0.38	4.5	4.9	4.4	4
86	25-09-14	10:35:03	121.37	22.77	15.4	5	0.02	2.7	3.5	2.8	4
87	26-09-14	4:21:24	95.23	12.52	20.2	5.5	0.04	1.2	1.2	1.1	7
88	26-09-14	16:16:00	124.44	13.7	38	5	0.1	1.8	0.9	1.1	4
89	27-09-14	15:15:43	94.2	5.05	50.2	5.2	0.01	1.9	1.1	2.8	5
90	30-09-14	16:45:56	67.74	1.6	10	5.5	0.6	3.9	6.3	1.9	13
91	03-10-14	8:05:44	122.12	11.33	19.4	5.5	0.02	1.2	2.2	3.9	8
92	07-10-14	13:49:40	100.47	23.38	8.5	6	0.12	6.1	2.9	2.2	14
93	12-10-14	3:32:46	93.87	12.87	136.3	5.2	0.15	1.4	1.3	3.7	10
94	14-10-14	18:36:06	94.24	7.56	10	5.1	0	2.9	1.2	0.8	3
95	16-10-14	0:56:31	97.22	1.05	26.8	5.3	0.01	4.9	2.7	5.2	6
96	16-10-14	8:34:50	93.49	3.99	34	5.4	0.54	5.9	8.1	6.2	11
97	17-10-14	9:26:00	107.17	-6.5	151.6	5.2	0.02	2.3	3	5.1	5
98	17-10-14	23:32:49	94.6	7.55	43	5.1	0.02	1.2	2.8	10	4
99	26-10-14	2:58:44	94.41	7.53	10	5	0.14	1.5	1.6	4.8	9
100	26-10-14	8:56:42	112.8	-10.24	36.1	5	0.02	1.4	2.7	1.2	3
101	30-10-14	12:11:37	117.55	-6.92	559.1	5.4	0.03	2.4	2.5	8.2	5
102	31-10-14	17:04:58	35.9	-5.42	10	5.3	0.01	3.3	5.4	2.2	5
103	02-11-14	0:58:11	94.3	7.39	30.3	5.4	0.59	12.4	12.2	19.4	10
104	06-11-14	15:46:20	94.33	7.42	28.8	5.1	0.27	1.9	1.5	0.4	8
105	07-11-14	0:20:47	95.07	4.78	39	5.4	0.05	1	0.6	0.4	5
106	10-11-14	2:39:03	69.56	-23.98	10	5	0.5	1.8	1.4	1.2	5
107	10-11-14	10:34:29	94.92	19.47	67.5	5	0.51	2.2	2.8	1.8	10
108	11-11-14	7:48:13	97.54	20.68	51	7	0.49	1	1.6	1.3	7
109	11-11-14	7:50:08	94.3	7.46	8	5.3	0.08	1.4	2.5	9.8	8
110	11-11-14	8:04:36	94.2	7.45	10	5.3	0.05	1	0.6	1	9
111	12-11-14	19:59:43	57.74	11.76	20	5.3	0.01	2.8	5.7	8.9	7
112	15-11-14	9:47:58	126.56	1.79	35	5.4	0.02	1.2	0.9	4.6	7
113	16-11-14	11:06:09	97.92	1.65	36	5.2	0.24	4.8	4.2	4.1	11
114	17-11-14	4:34:12	94.42	20.78	66	5.3	0.14	1.8	3.7	2.6	6
115	17-11-14	5:08:10	94.36	7.61	10	5	0.01	2.6	1.8	4.5	11
116	17-11-14	13:34:12	120.27	19.54	10	5.6	0.17	1.3	1.4	1.1	3
117	17-11-14	14:01:28	120.35	19.57	10	5.4	0.02	1.6	2.4	7.8	8
118	17-11-14	19:06:31	120.36	-7.06	589.4	5.5	0.03	1.4	1.4	6.1	7
119	18-11-14	3:25:37	94.36	7.48	6.6	5.6	0.47	1.5	1.7	1.4	12
120	18-11-14	6:06:25	94.38	7.45	10	5.1	0.28	1.9	1.9	1.3	5
121	18-11-14	9:14:47	120.48	19.53	10	5.3	0.53	4.7	3.8	14.7	12
122	18-11-14	9:15:54	120.42	19.47	10	5.4	0.03	2	1.9	5	6
123	19-11-14	5:03:11	68.13	-2.68	10	5.3	0.42	3.3	5.5	34.3	13
124	19-11-14	5:06:30	68.02	-2.72	10	5.3	0	4.2	2.9	35.1	5
125	20-11-14	9:48:20	120.62	23.31	8.7	5.7	0.02	1.1	1.9	8.7	7
126	21-11-14	3:29:11	120.07	20.65	4	5.7	0.24	4.9	4.6	4.3	4
127	24-11-14	15:30:09	96.16	2.77	46	5	0.48	3.8	5.3	4.8	5
128	25-11-14	5:19:54	61.29	5.74	10	5	0.04	3.1	3.7	4.8	5
129	26-11-14	13:08:39	61.34	5.83	10	5.2	0.03	0.8	1.7	2.6	7
130	27-11-14	0:18:28	61.3	5.81	10	5.7	0.54	1.8	1.4	1.2	6
131	28-11-14	1:18:46	92.8	12.51	43.8	5.5	0.01	1.4	2.7	5.2	3
132	28-11-14	12:42:10	121.37	2.21	44.3	5	0.02	1.8	1.7	7.7	4
133	28-11-14	13:23:16	61.33	5.75	10	5.4	0.17	1.6	2.3	2.6	7
134	29-11-14	13:05:09	61.38	5.73	10	5.3	0.4	1.5	1.4	1.5	8
135	29-11-14	15:36:16	121.47	19.93	30	5.1	0.02	2	1.9	5.5	5
136	29-11-14	19:54:27	61.37	5.82	10	5.1	0.01	1	1.9	2.9	11
137	30-11-14	5:48:22	61.38	5.78	10	5.1	0.03	4.5	2.2	3.7	4
138	30-11-14	18:03:01	90.09	3.41	21	5	0.05	1.6	3	4.5	5
139	01-12-14	3:47:49	61.37	5.91	10	5.2	0.3	2.1	3.6	3	6
140	01-12-14	16:37:21	123.82	2.93	10	6.3	0.45	3.1	5.3	4.4	6
141	01-12-14	22:47:27	67.7	1.6	10	5.4	0.42	3.3	4.5	4.3	13
142	02-12-14	4:53:45	61.3	5.97	13.2	5.4	0.07	1.5	1.6	1.6	8
143	02-12-14	5:11:31	123.13	6.16	614	6.6	0.12	0.8	1	2.5	6
144	03-12-14	0:27:04	122.42	-2.93	10	5.5	0.51	1.9	1.2	1.8	11
145	03-12-14	2:33:25	122.43	-2.87	48.5	5	0.02	2.4	3.9	22.2	11
146	03-12-14	14:19:10	122.48	9.63	10	7.4	0.02	21	10.8	5.8	12

(continued on next page)

Table 1 (continued)

S.No.	Date	Time	Longitude	Latitude	Depth (km)	Magnitude M _w	RMS (s)	ERX (km)	ERY (km)	ERZ (km)	N
147	04-12-14	10:53:32	65.17	-12	10	5.6	0.07	0.2	0.3	0.5	13
148	05-12-14	18:43:46	100.47	23.34	11	5.5	0.47	1.8	1.6	1.5	10
149	06-12-14	10:20:02	100.53	23.36	10	5.5	0.19	3.3	5.1	4.7	10
150	10-12-14	20:27:55	121.17	19.13	45.6	5.2	0.01	1.3	1.5	6.6	6
151	16-12-14	17:10:35	101.6	18.02	10	9.1	0.15	1.4	1.5	7.5	9
152	17-12-14	6:10:06	100.14	-3.83	10	6	0.35	1.6	2.3	4.5	10
153	17-12-14	15:24:30	95.79	2.75	33	5.2	0.03	0.3	0.5	1	8
154	19-12-14	14:41:45	94.62	6.88	37	5.1	0.03	0.2	0.4	0.8	11
155	21-12-14	16:59:03	100.74	19.73	190	5.7	0.03	0.9	0.7	3.6	9
156	29-12-14	9:29:37	121.52	8.63	8	6	0.02	2.3	1.4	17.6	13
157	29-12-14	12:09:36	125.61	2.75	174.8	5.1	0.19	4.6	4.3	2.6	4
158	31-12-14	9:26:22	120.67	13.75	110	5.5	0.03	1	1.2	6.6	9
159	31-12-14	19:47:36	33.86	-10.03	14.93	5.1	0.01	1.2	1.7	2.2	4
160	02-01-15	8:21:52	59.89	6.28	8	5.5	0.37	3.5	4.9	21.4	9
161	02-01-15	8:21:56	60.37	6.57	10	5.5	0.21	19.1	14	5.7	9
162	02-01-15	8:43:22	122.66	13.09	10	5.3	0.21	1.6	1.8	1.4	8
163	03-01-15	8:03:52	121.37	2.41	10	5	0.02	1.3	1.3	3.7	11
164	09-01-15	22:59:12	96.09	2.59	49.9	5	0.02	1.9	1	3.4	8
165	10-01-15	2:05:46	68.36	-5.66	10	5.6	0.03	0.4	0.6	1.2	13
166	10-01-15	19:32:00	120.25	14.77	59	5.8	0.04	2.5	2.6	1.5	9
167	12-01-15	0:19:57	66.33	-20.04	10	5	0.03	0.7	1	2.9	9
168	15-01-15	0:09:28	119.97	0.14	61.9	5.1	0.02	1.4	1.8	6.5	5
169	15-01-15	14:01:51	102.97	-4.49	58	5.1	0.56	4.2	4.2	13.7	10
170	17-01-15	5:09:18	120.63	13.97	134	5	0.03	0.9	1	7.9	8
171	18-01-15	0:27:22	120.69	13.93	149.8	5.2	0.03	0.8	0.9	5.1	8
172	19-01-15	17:19:46	119.76	4.61	11	5.5	0.02	0.6	0.7	2.6	10
173	23-01-15	20:35:34	60.75	-29.46	15.1	5	0.01	0.7	1	7.1	12
174	26-01-15	7:09:55	122.38	9.61	56.8	5.5	0.02	6.3	2.9	2.6	6
175	27-01-15	0:53:19	97.24	1.34	12.6	5.7	0.04	1.1	1.8	1.1	9
176	02-02-15	15:13:40	124.58	13.98	17	5.4	0.03	10	4.5	4.2	6
177	02-02-15	21:29:40	105.36	-6.12	43.2	5	0.19	1.9	1.7	9.1	9
178	04-02-15	17:41:45	124.99	-0.13	54.3	5.3	0.02	0.8	0.7	2.8	9
179	05-02-15	13:32:55	89.7	-21.81	10	5.1	0.02	0.7	1	1.4	9
180	08-02-15	15:09:08	119.45	-2.43	10	5.5	0.02	3.3	3.7	0.9	10
181	10-02-15	14:47:50	57.38	9.68	12	5.4	0.02	0.9	1.5	3.2	5
182	10-02-15	16:09:24	120.62	14	134.9	5.2	0.03	0.8	0.7	3	7
183	11-02-15	3:30:12	92.35	13.23	20.1	5.1	0.23	2.3	4.3	4.1	8
184	25-02-15	1:31:41	119.84	6.08	9	5.6	0.02	1.9	2.5	1.3	10
185	27-02-15	13:43:55	110.72	0.13	20	7.1	0.02	1.5	1.1	2.8	11
186	27-02-15	13:45:03	122.6	-7.55	572	7.1	0.02	0	3.2	1.6	5
187	28-02-15	10:53:04	118.82	-8.91	117.9	5.2	0.02	0.7	0.8	4.8	9
188	01-03-15	3:32:34	124.31	0.09	84	5.6	0.03	0.8	0.9	2	10
189	02-03-15	1:40:52	124.53	-0.05	71.5	5.7	0.02	0.7	0.6	3.7	10
190	03-03-15	10:37:32	98.84	-0.7	36.2	6.3	0.02	0.7	1	2.6	11
191	05-03-15	0:07:12	96.96	0.21	10	5.1	0.02	1.2	1.8	2.6	10
192	15-03-15	23:17:17	122.31	-0.54	31	5.9	0.02	0.8	0.9	6.1	9
193	15-03-15	23:17:18	122.4	-0.64	43.4	5.9	0.05	5.5	2.2	1.7	11
194	22-03-15	18:12:25	89.7	1.97	12	5	0.02	4.7	5.1	5.9	5
195	23-03-15	15:48:03	124.88	0.65	53.2	5	0.43	3.8	4.2	23.3	9
196	28-03-15	22:28:51	121.99	0.4	118	5.9	0.24	7.9	7.8	13.7	6
197	02-04-15	2:56:09	102.66	-4.46	61.5	5	0.03	0.8	0.7	2.9	9
198	09-04-15	22:49:43	92.85	14.07	27.9	5	0.02	1.6	2.8	3.5	8
199	10-04-15	16:23:04	65.86	-13.79	10	5.6	0.03	0.4	0.6	1	13
200	11-04-15	11:42:53	124.81	4.82	303	5.2	0.02	0.9	1.1	6.6	8
201	11-04-15	12:44:37	104.34	-6.65	35	5	0.02	1	0.9	5	8
202	19-04-15	5:32:15	66.58	-17.11	10	5.1	0.02	0.6	1.2	0.9	9
203	19-04-15	9:11:30	115.42	-3.68	10	7.7	0.01	3.1	22.1	11.9	3
204	19-04-15	18:40:25	98.96	1.9	122.7	5.4	0.02	0.8	1.1	3.7	11
205	20-04-15	9:05:32	102.66	-5.42	17	5.8	0.07	3.6	1.6	3.9	10
206	21-04-15	0:17:29	92.95	14.12	27.1	5.1	0.02	0.7	1.2	5.2	10
207	21-04-15	16:10:37	56.27	14.42	10	5	0.07	0	1.8	1.7	3.7
208	24-04-15	5:28:08	124.25	-0.2	79.4	5.3	0.02	1.1	0.7	3.5	8
209	26-04-15	10:38:00	120.41	-10.59	35	5.3	0.03	0.6	0.6	3.3	10
210	29-04-15	1:27:16	86.59	3.2	10	5.2	0.01	8.5	6.1	4.1	3
211	05-05-15	20:01:13	67.1	-15.41	10	5	0.02	7.3	3.9	1.3	5
212	05-05-15	20:24:26	67.27	-15.42	10	5.2	0.01	7.8	12.8	9.4	4
213	05-05-15	20:53:20	67.25	-15.3	11	5.5	0.03	0.6	1.1	0.9	10
214	08-05-15	3:12:21	97.81	1.54	38	5.7	0.63	5.3	7.3	13.6	10
215	11-05-15	17:42:02	67.83	-7.76	10	5.3	0.71	3.9	5.7	6.1	13
216	12-05-15	7:36:30	94.13	21.95	255	5.3	0.03	3.4	1.4	2.8	9
217	15-05-15	20:26:55	102.27	-2.48	159	6	0.02	0.9	1.4	3.2	9
218	18-05-15	5:49:12	66.77	2.41	10	5.1	0.02	0.7	1.4	5.9	8
219	30-05-15	6:48:29	43.16	11.69	7.3	5	0.46	4.8	4.7	5.1	9
220	01-06-15	14:07:50	95.57	4.65	73.5	5	0	1	1.3	23.8	9

(continued on next page)

Table 1 (continued)

S.No.	Date	Time	Longitude	Latitude	Depth (km)	Magnitude M _w	RMS (s)	ERX (km)	ERY (km)	ERZ (km)	N
221	04-06-15	23:15:42	116.59	6.03	15	6	0.03	2.1	3.1	1.1	10
222	08-06-15	10:47:21	68.01	-2.52	10	5.4	0.25	2.5	3.4	4.5	11
223	10-06-15	22:01:30	120.73	-10.52	35	5.1	0.02	0.7	0.9	5.3	8
224	12-06-15	18:29:16	116.68	6.21	7.2	5.2	0.02	0.8	1.1	3.7	7
225	13-06-15	5:03:44	120.69	13.81	137.2	5	0.02	0.7	0.7	4.1	9
226	25-06-15	1:21:25	40.5	17.46	11.6	5.1	0.02	1.5	1.7	4.3	8
227	02-07-15	7:04:32	120.22	-7.45	413.4	5.2	0.03	1.2	1.3	3	11
228	03-07-15	3:16:35	95	11.41	24	5.5	0.02	0.6	1.1	0.8	10
229	03-07-15	3:57:40	91.58	21.46	10	5.9	0.02	0.6	1.1	0.8	10
230	04-07-15	0:44:38	56.39	14.36	10	5.2	0.03	1.3	2.7	4.1	6
231	08-07-15	0:38:56	94.73	4.99	34.3	5	0.02	1.2	1.5	4.2	7
232	13-07-15	11:14:04	46.37	11.94	14.3	5.3	0.02	0.8	1.3	4.4	7
233	13-07-15	16:52:28	46.21	12.09	10	5.1	0.02	0.8	0.8	4.2	6
234	15-07-15	14:10:04	41.05	-15.61	14.6	5.1	0.02	0.9	1	5.3	6
235	21-07-15	5:49:22	90.23	19.19	10	5.1	0.01	3.6	4.3	3.7	3
236	22-07-15	5:35:22	93.97	3.68	10	5.4	0.02	2	3.8	1.6	5
237	23-07-15	13:17:44	66.79	-14.9	10	5	0.03	1.7	4.6	2.5	8
238	24-07-15	21:44:37	109.03	-7.93	50	5.5	0.02	1.8	2.5	2	4
239	26-07-15	7:05:05	113.07	-8.9	10	5.3	0.05	2.6	2.8	1.6	10
240	31-07-15	22:26:07	118.3	-8.17	10.3	5	0.02	1.2	1.7	2.7	9
241	02-08-15	13:08:46	123.85	8.18	602.9	5	0.02	1.2	2.1	5.8	7
242	06-08-15	5:05:43	116.3	-9.74	10	5.6	0.02	1.6	0.9	4.2	7
243	06-08-15	10:08:55	98.92	1	77.9	5	0.03	1	1.5	5.6	9
244	09-08-15	4:35:11	121.17	19.68	10	6	0.03	3.8	1.8	1.3	8
245	15-08-15	8:19:31	101.92	-3.54	56	6.8	0.02	4.1	1.7	2.9	9
246	17-08-15	16:16:59	51.78	13.71	10	5.6	0.02	1.6	4.4	2.7	4
247	25-08-15	3:29:33	93.32	5.02	14.9	5	0.01	3.5	3.8	10.2	6
248	29-08-15	20:02:27	116.34	-10.84	34.4	5	0.02	0.9	0.8	2.7	6
249	02-09-15	1:13:50	53.49	14.26	12	5.3	0.02	0.8	1	3	8
250	02-09-15	7:20:31	53.78	14.18	29	5.2	0.02	5.7	8	4.1	4
251	04-09-15	20:08:32	107.22	-8.04	37	5.4	0.03	6.5	1.9	2.4	7
252	09-09-15	1:15:55	120.78	13.75	134.4	7.3	0.02	0.9	1	3.9	7
253	12-09-15	23:39:19	122.05	-0.74	18.2	5	0.02	0.7	0.8	2.2	8
254	13-09-15	1:12:50	124.96	-0.11	10	5.5	0.02	3.6	3.8	3.3	5
255	17-09-15	4:02:23	86.2	14.34	10	5	0.03	1.1	1	3.3	6
256	23-09-15	16:18:18	105.05	-7.81	10	6.8	0.03	10.4	3.9	3.2	6
257	25-09-15	7:53:46	97.87	20.01	35	5.5	0.05	0.9	0.9	3.4	9
258	26-09-15	3:09:27	105.42	21.95	647	5.4	0.03	0.6	1.1	0.9	11
259	26-09-15	17:23:27	123.8	5.26	516	5.5	0.01	0.7	1	2.6	10
260	01-10-15	0:05:01	103.71	-6.03	34	5.3	0.01	4.5	2.6	3.4	8
261	01-10-15	2:49:53	103.64	-6.08	35	5	0.01	3.1	3.8	1.4	7
262	03-10-15	9:43:59	70.82	-26.24	10	5.4	0.27	3.9	5.5	9.6	10
263	09-10-15	16:28:25	123.89	-0.02	96.3	5	0.28	2.9	3	15.7	8
264	10-10-15	4:04:37	97.65	14.93	10	7.5	0.03	5.5	4	3.5	6
265	10-10-15	9:04:01	107.4	-8.05	35	5.3	0	0	6.5	1.7	0
266	11-10-15	7:27:37	97.03	18.32	341	7.1	0.02	0.9	1	4.3	6
267	19-10-15	13:50:42	120.62	13.87	106	5.8	0.01	4.3	2.2	11.3	5
268	22-10-15	0:32:28	74.06	-27.77	10	5.2	0.03	0.6	1	1.6	10
269	22-10-15	7:50:30	74.03	-27.87	10	5.2	0.04	0.7	1.2	0.9	10
270	26-10-15	10:09:06	97.06	-1.45	21	5	0.03	0.4	0.8	1	10
271	27-10-15	12:15:21	67.07	-16.31	10	5.3	0.21	1.3	2.2	4.4	11
272	31-10-15	4:43:56	124.06	-9.06	53.7	5.1	0.02	1.1	2	2.6	4
273	04-11-15	3:44:30	124.2	-7.34	46	5.9	0.01	1.5	1.6	5.1	5
274	04-11-15	6:14:33	105.05	-6.75	10	5.1	0.01	1.5	1.6	5.1	9
275	04-11-15	8:12:14	98.04	0.58	28.9	5.3	0.02	7.8	6.2	3.4	5
276	05-11-15	16:24:14	124.8	-8.22	20.2	5.7	0.02	4.3	2.7	4.7	4
277	07-11-15	19:40:14	119.85	16.49	37	5.4	0.03	1.2	2.7	3.9	7
278	07-11-15	20:57:52	111.2	-10.18	10	5	0.03	2.9	4.1	3.3	5
279	08-11-15	9:34:38	98.72	-0.62	23	5.4	0.03	3.8	1.4	2.5	8
280	08-11-15	10:42:02	94.55	6.88	8	5.4	0.03	1.2	2	2.3	10
281	08-11-15	11:54:39	94.61	6.79	10.1	5.2	0.03	1.3	4.7	6.4	4
282	08-11-15	11:54:41	94.52	6.92	34	5	0.01	3.9	2.7	17.5	11
283	08-11-15	14:34:05	94.44	6.68	10	5.3	0.03	0.9	1.8	1.1	7
284	08-11-15	16:47:02	94.65	6.84	10	6.4	0.03	0.8	1.3	2.3	10
285	08-11-15	16:59:11	93.4	6.7	10	8	0.02	0.8	1.7	4.4	9
286	08-11-15	19:14:47	94.53	6.98	10	5.6	0.03	2.5	3.7	3.5	7
287	09-11-15	6:12:14	94.88	6.52	11.8	5	0.04	0.8	1.6	1.6	8
288	09-11-15	8:12:46	94.8	6.41	10	5.5	0.38	3.2	6.2	13.7	10
289	14-11-15	16:53:31	94.57	6.88	26	5	0.14	2.5	2.9	2.9	6
290	16-11-15	5:04:47	87.41	13.38	10	6.1	0.02	3.8	6.3	40	5
291	17-11-15	19:07:43	119.13	-8.31	25.1	5.5	0.02	1.4	2.3	5.8	3
292	18-11-15	16:46:55	104.11	-7.31	10	5	0.03	2.5	3.3	9.4	3
293	27-11-15	8:33:58	94.84	22.5	11.4	5.3	0.02	0.5	0.9	1.6	10
294	27-11-15	15:46:26	95.99	1.82	16	5.1	0.02	1.7	1.1	3.6	8

(continued on next page)

Table 1 (continued)

S.No.	Date	Time	Longitude	Latitude	Depth (km)	Magnitude M _w	RMS (s)	ERX (km)	ERY (km)	ERZ (km)	N
295	28-11-15	13:11:39	59.53	15.23	10	5.4	0.03	0.4	0.7	0.7	13
296	28-11-15	14:47:19	106	-7.05	51.3	5.3	0.03	2.8	1.8	12.4	6
297	30-11-15	20:19:05	67.7	-8.79	10	5.5	0.76	4	6.5	6.4	9
298	11-12-15	3:20:48	102.97	-4.96	48.6	5.1	0.01	1	1.1	3.2	6
299	19-12-15	15:03:36	107.02	-8.37	27	5.7	0.03	2.3	1.2	4.3	9
300	20-12-15	18:47:36	117.64	3.65	14	6.1	0.03	1.3	1.6	3.5	11

Table 2

Historical Tsunamis occurred in The Indian Ocean region.

S. No.	Date	Place	Latitude	Longitude	Magnitude M _w	Depth (Km)	References
1	April 11, 2012	Off-West Coast Sumatra, Indonesia	2.327	93.063	8.6	20	Yadav et al. (2013)
2	December 26, 2004	West coast of Sumatra, Indonesia	3.4125	95.9012	9.1 / 9.3	30	McCloskey et al. (2005)
3	13 September 2002	Diglipur, Ariel Bay, North Andaman Island	13.036	93.068	M _s 6.8	21	Rajendran et al. (2003)
4	June 2, 1994	South Coast of Java, Indonesia	-10.477	112.835	7.2	18	Abercrombie et al. (2001)
5	August 19, 1977	Southwest coast of Sunda Island, Indonesia	-11.085	118.464	8.3	33	Kenji and Yoshinobu (1995)
6	November 10, 1942	Southwest Indian Ocean regionRidge	-49.92	30.336	8.3	10	Okal and Stein (1987)
7	26 June 1941	Andaman and Nicobar Islands	12.5	92.5	8.1	55	Jhingran (1952)
8	31 December 1881	Nicobar Island	8.520	92.430	7.9	NA	Ortiz and Bilham (2003)
9	November 25, 1833	Sumatra Fore Arc, Indonesia	-2.500	100.500	8.8-8.3	75	Newcomb and McCann (1987)

areas ([Mishra et al., 2011](#)), impacting both urban and rural population. The outcome of this study may be benefitted to the latest research in the field of seismology to address its societal impacts, because it provides essential information for the seismic hazard evaluation of the region.

2. Geology and tectonics of the study area

The Indian Ocean region ([Fig. 1](#)) is geologically the youngest and physically complex in its tectonic setting. The complex tectonic province attributed to several factors such as subduction, arc (parallel, transformed, reverse) faults, fracture, arc volcanism, and the spreading ridge, back-arc rift zone ([Demopoulos et al., 2014](#)). The formation and origin of the Indian Ocean are due to the motion of the tectonic plates formed about 140 million years ago (<https://www.basicplant.com/inian-ocean>) and (<https://www.pubs.usgs.gov/imap/0380/report.pdf>). The Indian Ocean region is constrained by Iran, Pakistan, the Malay Peninsula, the Sunda Island of Indonesia, on its north, east, south and west it is bounded respectively by India and Bangladesh; Australia; Antarctica; Africa and the Arabian Peninsula (<https://www.britannica.com/place/Indian-Ocean>). The Indian Ocean mingles with the Atlantic Ocean in the south of Africa and to the east and the Pacific Ocean in the southeast. The study region comprises of marginal sea (Arabian Sea to the northwest, and the Andaman Sea to the northeast, Bay of Bengal), ridges and Fractured Zone (Arabian Plate called the Owen Fracture Zone, Carlsberg Ridge, Chagos-Laccadive, Mid-Indian (Central Indian) Ridge, Broken Ridge, Ninetyeast Ridge), the basin (Arabian, Somali, Madagascar, Mid-Indian basin, Wharton, north Australia basins, Cocos, Andaman), trenches (Vema, Chagos and Java, Sunda Trench), the north and the central Indian Ocean, the Bay of Bengal, Arabian Fan across of Ninetyeast Ridges and Ninetyeast Ridges ([Kanayev et al., 2017](#)). The mid-ocean ridges in the Indian Ocean region comprise of Carlsberg ridge (CR), Central Indian Ridge (CIR), Southwest Indian Ridge (SWIR), and Southeast Indian Ridge (SEIR) systems. These CIR, SWIR and SEIR meet at the Rodriguez Triple Junction (RTJ) forming an inverted Y shaped ridge system ([Fig. 1](#)), which contain a variety of sediments, and the fracture zones cut by numerous north-north-east's trending at this Mid-Indian Ridge ([Souriau, 1981](#)). The materials in the Indian Ocean are (1) elastically hard rocks (volcanic and limestone) on topographically elevated areas in the Mid-Indian Ridge (2) deep basins is

having abundance of manganese nodules (3) primarily all coastal areas is predominant of ilmenite placers (4) adjacent to the Indonesian Archipelago, the eastern Indian Ocean is filled with silicic volcanic ash ([Qasim, 1999](#)).

Several studies have been made by different researchers that the eastern plate of the Indian Ocean shows an oblique convergence across the Burma-Andaman arc (e.g., [Fitch, 1970](#); [Verma et al., 1978](#); [Curry et al., 1979](#), [Mishra et al., 2011](#)). There is great earthquake rupture between the boundary of Indo-Australian plate in 2004 and 2005. This great earthquake moves the Indo-Australian plate towards northward with speed 40–50 mm/year, and the portion of southeastern of the Eurasian plate segmented into the Burma and Sunda sub-plates ([Fig. 1](#)) ([Lay et al., 2005](#)). The plate boundary extends southward through Myanmar, remaining offshore as a subduction zone along the Andaman–Nicobar Islands south to Sumatra, where it turns eastward along the Java trench. The nature of convergence contrasts from continental type in the Burmese arc to oceanic type in the Andaman arc. West of the Island arc is the Andaman-Nicobar trench; it is linked with the Sunda Trench in the south. The trench is a dormant feature of Andaman-Nicobar Islands and the sediments filled by Bengal-Nicobar fan. The Burma sub-plate, often referred to as an overriding silver plate or subduction fault zone, constitutes the western section of the main Sunda plate. Oblique convergence of the Indian plate develops arc parallel strike-slip faults all along the edges of the silver plate, which is also deformed in strips, as the sub-plate drives over the subducted Indian plate ([Curry et al., 1982](#); [Curry, 2005](#), [Mishra et al., 2011](#)). The prominent tectonic structures in the region are: in the north, the north-south orientation of Indo-Burma ranges; in the south, the Andaman-Nicobar Islands; in the southeast, the Sumatra fault system. These zones have series of thrusts/faults; the West Andaman fault is the most conspicuous all across the Andaman-Nicobar Islands. Thus, the Andaman sea basin is considered to be a complex backarc-spreading center. The western fringe is marked with the Arakan-Yoma accretionary subduction complex. The western area of Andaman Sea is poised of Andaman-Nicobar Trench and accretionary subduction complex ridges ([Curry et al., 1979](#); [Mishra et al., 2011](#)). The West Andaman Fault (WAF) is the most prominent all along the Andaman-Nicobar Islands, which seems to be incessant from west-off of northern Sumatra to where it is disappeared beneath the terrigenous fill of the Irrawaddy-

Table 3
Detailed information on seismographic stations with their site characteristics. (GSN Network site).

Zone	Name of Stations	Station Code	Latitude	Longitude	Elevation	Site Geology
Zone I (Triple point junction)	Bukit Timah Dairy Farm, Singapore West Island, Cocos (Keeling) Islands Pallekele, Sri Lanka	BTDF COCO PALK	1.36 −12.19 7.27	103.77 96.83 80.7	64 1 460	NA Coral and limestone. Predominantly migmatite
	Qiongzhong, Hainan Province, China	QIZ	19.03	109.84	240	Geology: Granite Vault Conditions: Seismometers are located in a surface vault on concrete piers which are isolated from the floor and attached to bedrock (granite). Vault temperature varies by about 10°C over the year. A dehumidifier is required.
						Metamorphosed and crystalline limestone. The station is located on the edge of the eastern escarpment of the Matina Anticline. The Matina Anticline consists of coralline recent limestone already metamorphosed and even crystalline.
						Limestone interbedded with mudstone.
Zone II (Spreading Zone)	Davao, Philippines	DAV	7.07	125.58	151	Vault Conditions: KS54000 borehole depth is −102 m. CMG3-TB borehole depth is −9.0 m. Seismometer is located on the Pre-Cambrian shield known as Yilgarn block which consists of granite and granite gneiss. The age of the granite is about 2500 m years. The site is in the south-west corner of the block, 230 km from the southern boundary and coast, and 130 km from the western boundary which is the Darling Fault. Site is 150 km from the west coast.
	Kappang, Sulawesi, Indonesia Marble Bar, Western Australia Narrgin, Australia	KAPI MBWA NWAO	−5.01 −21.16 −32.93	119.75 119.73 117.24	300 190 380	Gneiss
						Granitic gneiss derived from rocks of Toro and Karagwe-Ankolean ages.
						Granite
Zone III (Prominent Fault)	Kilima Mbogo, Kenya Mbarara, Uganda Mahe, Seychelles	KMBO MBAR MSFY	−1.13 −0.6	37.25 30.74	1950 1390	Jurassic dolerite.
	Sutherland, South Africa	SUR	−32.38	20.81	475	Granite
	CHTO - Chiang Mai, Thailand	CHTO	18.81	98.94	420	Vault dug into a dike consisting of mafic rock
	Mt. Furi, Ethiopia Ar Rayn, Saudi Arabia Univ. of Sharjah, United Arab Emirates	FURI RAYN UOSS	8.9 23.52 24.95	38.68 45.5 56.2	2570 631 284.399	Late pre-Cambrian granodiorite, decomposed at surface. Vault Conditions: Sensors are located in a subsurface tunnel vault on two concrete piers that are isolated from the concrete flooring of the tunnel.
Zone IV (Volcanic and Hotspot)	Ambohimpanompo, Madagascar Diego Garcia, Chagos Islands, Indian Ocean	ABPO DGAR	−19.02 −7.41	47.23 72.45	1528 1	Site Description: The site consists of a recording building, shaded car park, and a tunnel vault surrounded by a chain link fence.
	Lusaka, Zambia	LSZ	−15.28	28.19	1200	Coral
	Lobatse, Botswana, Africa	LBTB	−25.02	25.6	1128	Granite
						Granite
Zone V (Subduction Zone)	Ambolihipanompo, Madagascar					
	Diego Garcia, Chagos Islands, Indian Ocean					
	Lusaka, Zambia					
	Lobatse, Botswana, Africa					

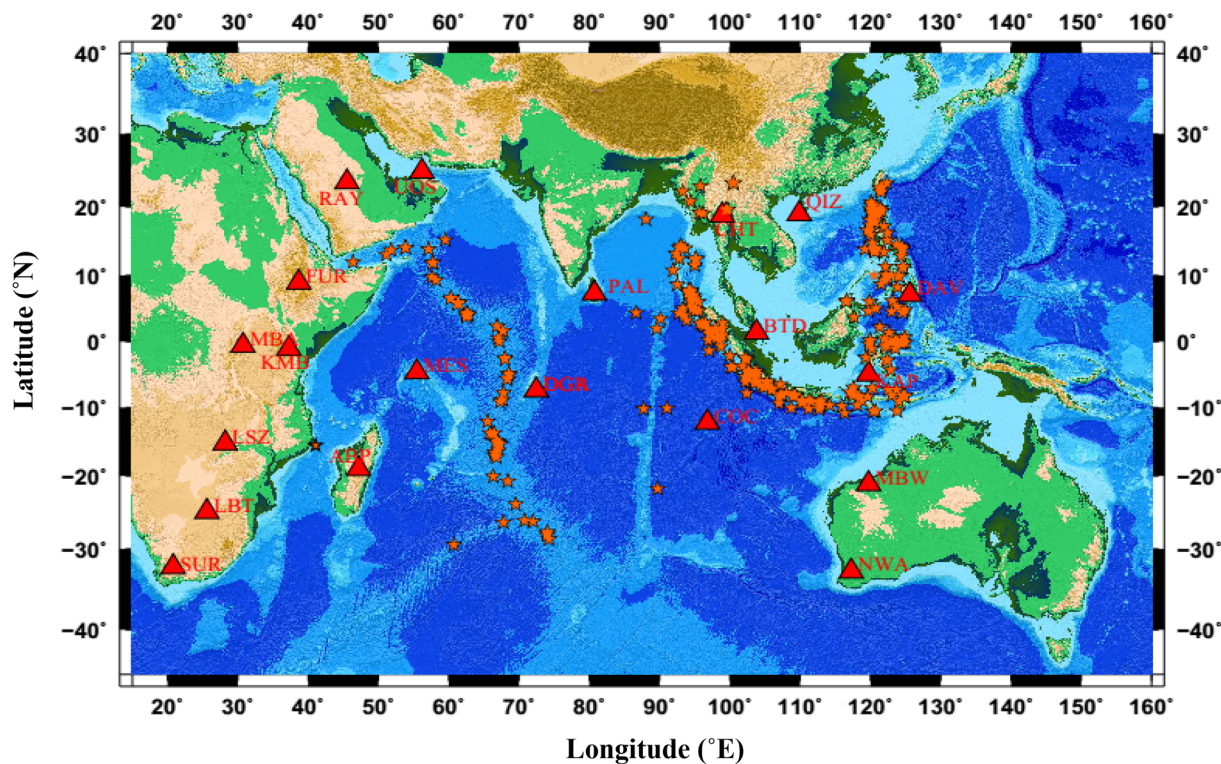


Fig. 2. A map of the study region with distribution of earthquake epicenters (red stars) and seismic stations (red triangles) used in this study. (For interpretation of the references to colour in this figure legend, the reader is referred to the web version of this article.)

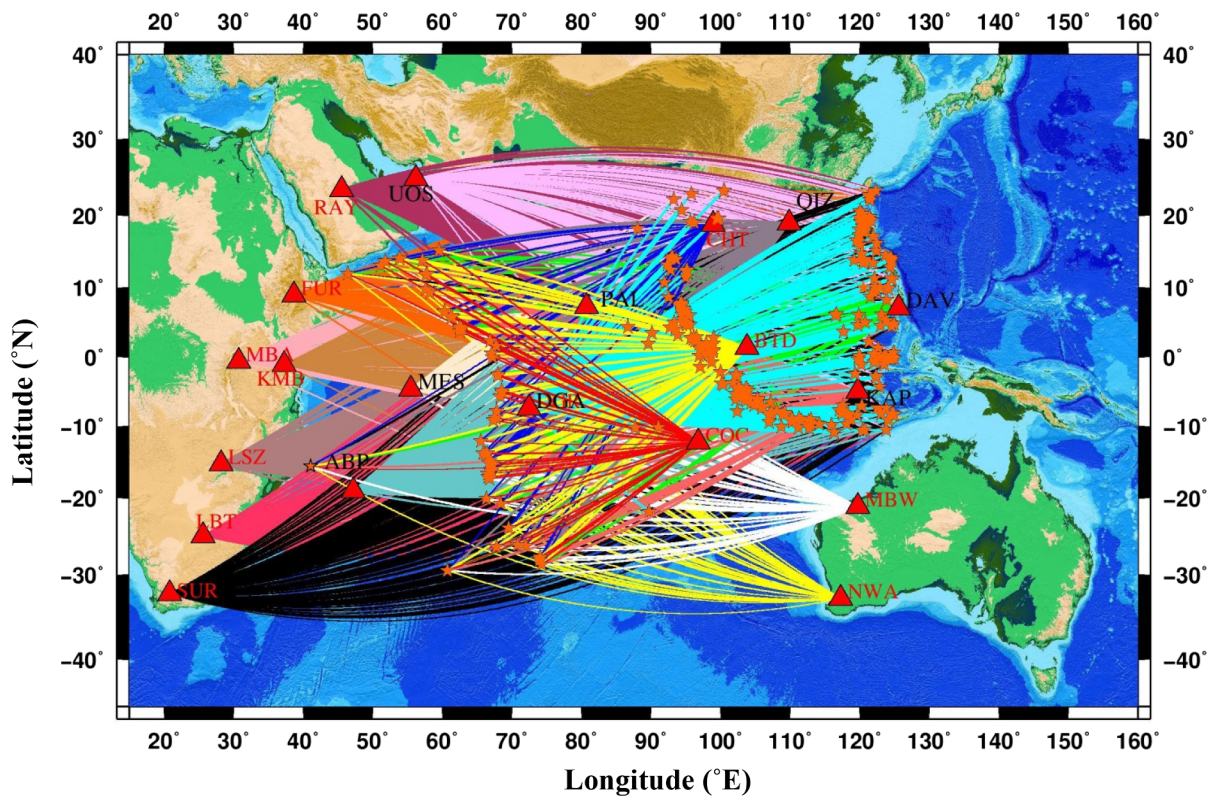


Fig. 3. The wave propagation paths used in the present study having earthquake epicenters (red star) and seismic stations (red triangle). (For interpretation of the references to colour in this figure legend, the reader is referred to the web version of this article.)

Table 4

Various central frequencies with low-cut and high-cut frequency bands used for filtering in the present analysis.

Low cut-off (Hz)	Central Frequency (Hz)	High cut-off (Hz)
1.00	1.5	2.00
2.00	3.00	4.00
4.00	6.00	8.00
6.00	9.00	12.00
8.00	12.00	16.00

Martaban (Curry et al., 1979; Mishra et al., 2011). Focal mechanism studies indicate that WAF is a north-south-oriented dextral strike-slip fault (Fitch, 1970). Further east, the line of this fault is marked by the vicinity of volcanic islands (Barren and Narcondum) and seamounts (Alcock and Sewell). The interior volcanic arc forms a belt with asymmetrical submarine ridges of volcanic seamounts and Barren and Narcondam with andesite volcanoes (Hamilton, 1979). A thorough overview of the historical seismicity can be found in Bilek and Engdahl (2007), Dewey (2007), and the tectonics of the area has been presented in the study by Mishra et al. (2007a). The Narcondam was extinct for the ages, and it witnessed smoke emission in June 2005 after a period of about six months from the 26 December 2004 mainshock. The Barren volcano erupted in March 1991 from dormant phase of about two centuries (Halder, 1992). The recent lava eruption of Barren volcano on 28 June 2005 after a series of aftershocks has generated interest among seismologists and volcanologists to explore and justify the inter-relationship between the earthquake-generating processes and volcanic eruption (Mishra et al., 2007b). Along the Burma Trench towards northward dragging of the dipping Indian lithosphere have activity due to active subduction (Le Dain et al., 1984). This evidence suggests a transition in the tectonic structure, and the low seismic activity in the central portion.

The earthquakes distribution showed a maximum concentration over the subduction zone where the oceanic plate is subducting underneath the continental plate. The tectonic features are connected with "dip-slip" types of vertical crustal movements along thrust faults (Bilham and Wallace, 2005). They have the potential of producing very destructive tsunamis in this entire region of the Andaman Sea due to its tectonic settings (Jhingran, 1952) that got indicated by occurrence of the larger rupture dimension due to 26th December 2004 tsunamigenic earthquake (Mw 9.3) (Mishra et al., 2007a,b). Most of the historic earthquake that occurred in the Indian Ocean province is given in Table 2, suggesting that this study of attenuation structure of the Indian Ocean region may furnish detailed information on different seismogenic layers to assimilate 1-D Velocity model that can be used as an initial model for obtaining 3-D seismic structure beneath the Indian Ocean for the further study.

3. Methodology

Aki and Chouet (1975) formulated single backscattering method to estimate Q_c at various frequencies. The seismic coda wave Q_c are backscattered waves, which generates from randomly distributed several heterogeneities that existing in the earth's rigid crust and upper mantle. This can be understood as a multiple scattering, due to diffusion process. Moreover single scattering provides information of outgoing wave before approaching the receiver that scatter only once and leading to a weak process. The coda wave at short lapse time (< 100 sec) are due to single scattering while long lapse time (> 100 sec) is due to multiple scattering (Kopnichev, 1977; Gao et al., 1983a,b). Under this hypothesis, the coda wave Q_c amplitude $A(f, t)$ at central frequency of interest f for a narrow band-width signal and at t lapse time that is measured from the origin time of the earthquake, as (Aki, 1980):

$$A(f, t) = S(f) t^{-\sigma} \exp\left(\frac{-\pi f}{Q_c}\right) \quad (1)$$

where $S(f)$ is the source function at frequency f and is considered as constant, σ is the geometric spreading factor and its value is 1.0, 0, 0.5 for spherical, plane body wave and surface wave respectively, and Q_c is the quality factor represents the average attenuation characteristics of the medium. Taking natural logarithm on both side of equation (1) and the equation in the form:

$$\ln[A(f, t)] = \lambda - m \quad (2)$$

where $\lambda = \ln S(f)$; and $m = \frac{\pi f}{Q_c}$. Eq. (2) represents slope of the straight line with slope $m = \frac{\pi f}{Q_c}$ provides the Q_c value at central frequency of interest " f " for the Indian Ocean. The frequency dependent relation given in the form $Q_c = Q_0 \left(\frac{f}{f_0}\right)^{\theta}$ is fitted for Q_c of each station, where the Q_0 is value Q_c at frequency (f_0) of 1 Hz and the frequency relation parameter " θ " reflect the degree of tectonic activity of the study area. In this case, the frequency parameter is close to 1 (Aki, 1981). Using a linear regression on left side of equation (2) versus t , to estimate value Q_0 and θ and hence Q_c can be determined from the slope of the fit. The methodology used in this study has wide scale applicability to diverse tectonic regions such as NW Himalaya (e.g., Scherbaum and Kisslinger, 1985; Jin and Aki, 1988; Havskov et al., 1989; Eck, 1988; Akinci and Eyidoğan, 1996; Gupta et al., 1998, 2012; Paul et al., 2003; Mak et al., 2004; Sharma et al., 2008; Parvez et al., 2008; Mohamed et al., 2010; Dobrynina 2011; Singh et al., 2012; Boulanouar et al., 2013; Gholamzadeh et al. 2013; Vandana et al., 2015; Das et al., 2018; Kumar et al., 2016; Singh et al., 2018).

4. Data-set and analysis

The earthquake data-set consists of 300-digital seismogram recorded by three-component broad-band seismometer around the placed Indian Ocean during the period from 01 January 2014 to 31 December 2015. The earthquake data-set is taken from the IRIS network having magnitude ($M_w \geq 5$), epicentral distances > 1000 km and depth from 0 to 600 km (Table 1). All events were measured digitally by three-component seismometers at sampling rate of 100 samples / second. The distant earthquake data are collected through this network for the study of subsurface structure and seismotectonic topographies of the Indian Ocean provinces. Most of the great earthquake occurred across the subduction zone where the Indo-Australian plate subducting underneath the Sunda plate forming "oblique subduction", across Great Sumatran fault and around spreading zone (e.g., Kayal et al., 2004; Mishra et al., 2007a,b; Padhy et al., 2011). The details of hypocentral parameters of earthquakes used in this study with their errors are listed in Table 1. The epicenters of the earthquake events are shown in Fig. 2. The details of seismographic stations with site characteristics are given in Table 2. The events used for the study region showed coda wave path coverage of the Indian Ocean region (Fig. 3).

The digital data-set are collected from all the 15-stations that have been converted to Seisan format using conversion code with the help of SEISAN software (Havskov and Otemöller, 2003). The HYP is the general program for hypocenter location and is based on HYPOCENTER (e.g., Lienert et al., 1986; Lienert and Havskov, 1995). The program is used for all common crustal and global phases, and also to locate teleseismic events using the velocity model of IASP91 model. The velocity of P-wave and S-wave considered is 7.72 km/sec and 4.42 km/sec respectively (Singh, 1988), which was used to study entire Indian Ocean. The epicenter location of earthquake events is shown in Fig. 2. For the analysis, the waveforms with low signal to noise ratio (SNRs) greater than 5 are used for the analysis. Moreover, the correlation coefficients are considered as a second assortment criterion, because Q -value with insignificant correlation coefficients leads to a poorly controlled Q - f relation and consequently less consistent estimate of Q_0 value. It

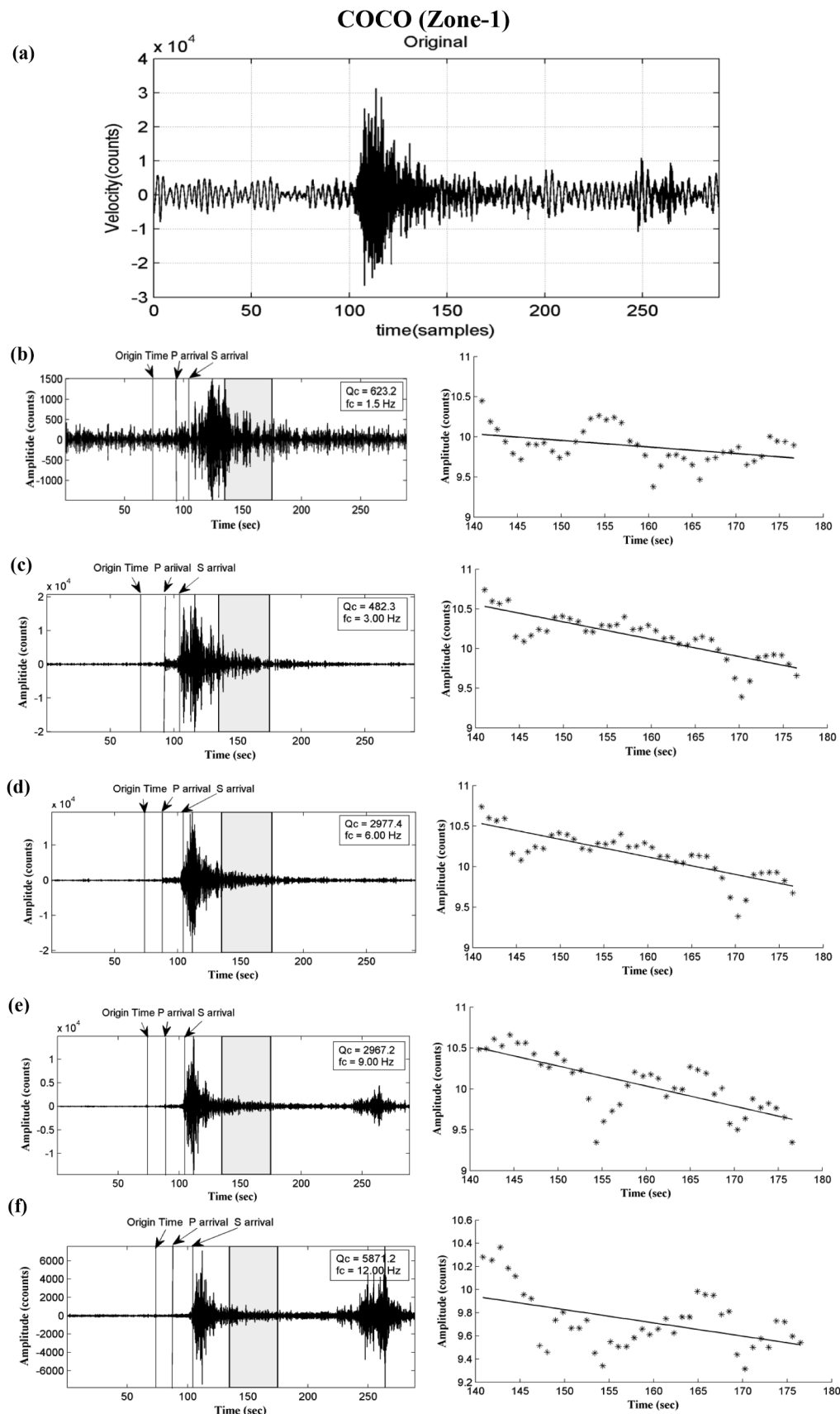


Fig. 4. (a) (Zone-1): An original plot of event of seismograms for one of the station COCO recorded on 10-02-2015. (b–f) Plot of band-pass filtered seismogram of the P, S, and coda wave portion recorded at the station with central frequency (C. F.). The best fitted linear line and estimated Q_c value for each central frequency are also shown in the figure. The coda waves portion of 40 s lapse time window length is indicated by grey window. Abbreviations P, P-wave arrival times; S, S-wave arrival time. Different zones are shown in Fig. 11.

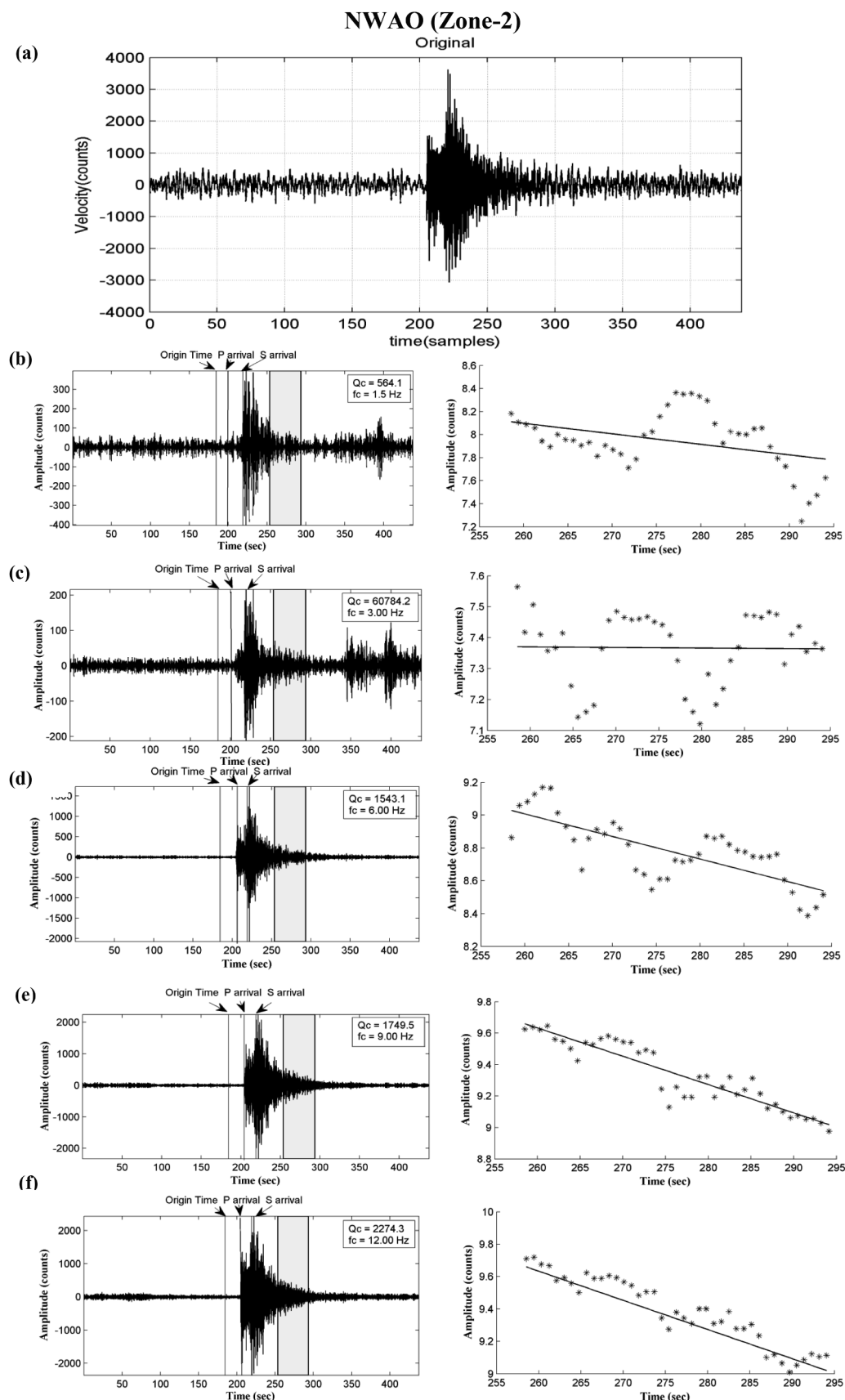


Fig. 5. (a) (Zone-2): An original plot of event of seismograms for one of the station NWAO recorded on 25-09-2014. (b–f) Plot of band-pass filtered seismogram of the P, S, and coda wave portion recorded at the station with central frequency (C. F.). The best fitted linear line and estimated Q_c value for each central frequency are also shown in the figure. The coda waves portion of 40 s lapse time window length is indicated by grey window. Abbreviations P, P-wave arrival times; S, S-wave arrival time. Different zones are shown in Fig. 11.

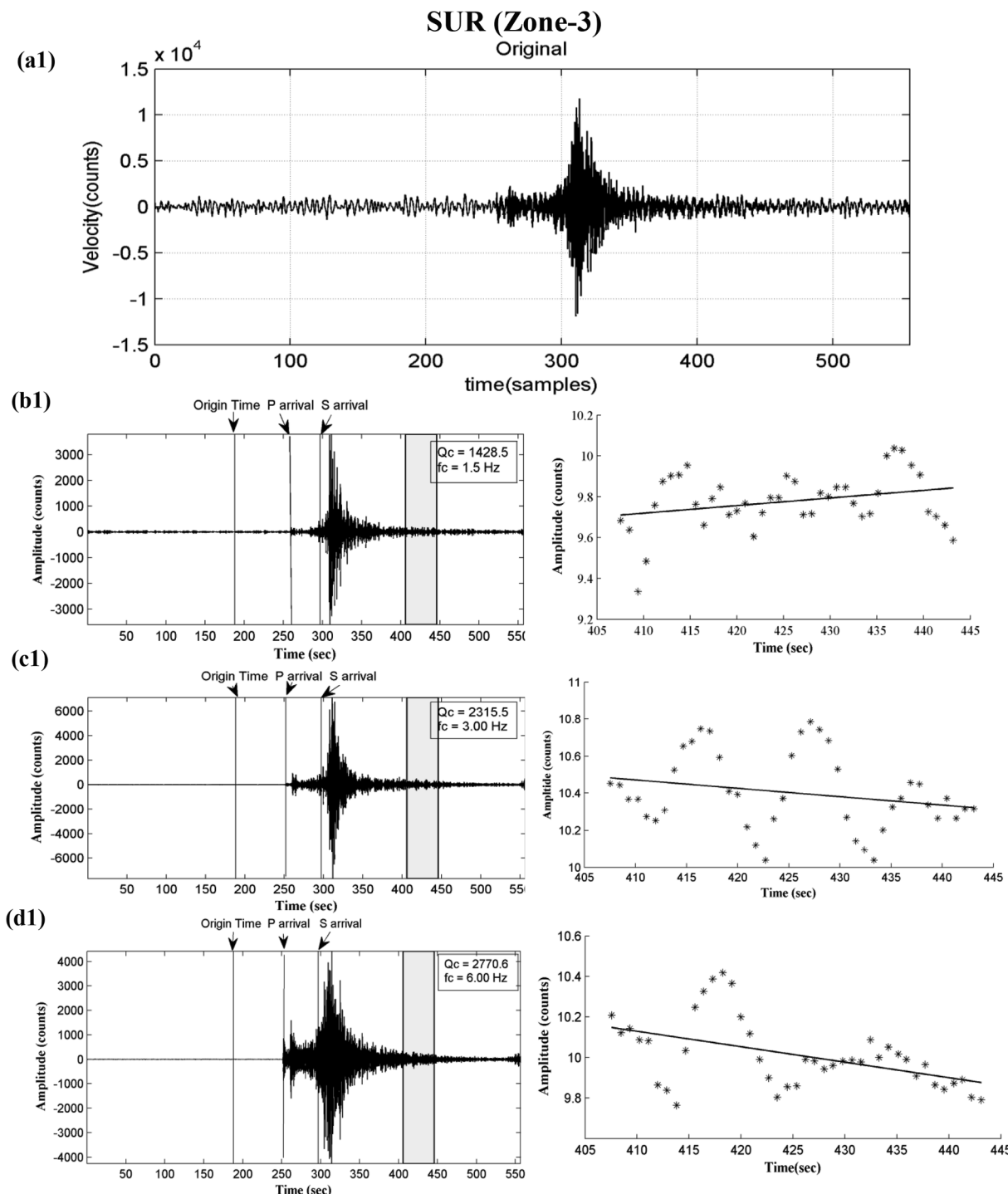


Fig. 6. (a1–a3) (Zone-3): An original plot of event of seismograms for one of the station SUR, MBAR and KMBO recorded on 28-11-2014, 02-02-2014 and 11-11-2014. (b1–f3) Plot of band-pass filtered seismogram of the P, S, and coda wave portion recorded at the station with central frequency (C. F.). The best fitted linear line and estimated Q_c value for each central frequency are also shown in the figure. The coda waves portion of 40 s lapse time window length is indicated by grey window. Abbreviations P, P-wave arrival times; S, S-wave arrival time. Different zones are shown in Fig. 11.

is suggested that to obtain the reliable values of Q_c correlation coefficient should be 0.7. The arrival of P-wave and S-wave are used to estimate the origin time and coda arrival times. Further Butterworth filter has been used as band-pass filter to the seismograms at five frequency band viz., 1–2; 2–4; 4–8; 6–12 and 8–16 Hz (Table 4). The contamination caused by direct S-wave has been eliminated by selecting the start time of coda window from earthquake origin time as twice of travel time of S-wave (Rautian and Khalturin, 1978) and travel time of

S-wave is computes from the travel-time table National Seismic Bureau of China (1980) (Mak et al., 2004). Due to variation of tectonics complexities and degree of complexity of the Indian Ocean region, the average frequency dependent attenuation relationships has been estimated at each filtered seismogram using five various lapse time windows (LTWs) 20, 30, 40, 50, and 60 s (Rautian and Khalturin, 1978).

The envelope of considered signal is evaluated from (RMS) root mean square values of coda amplitude from a moving window of 2 s

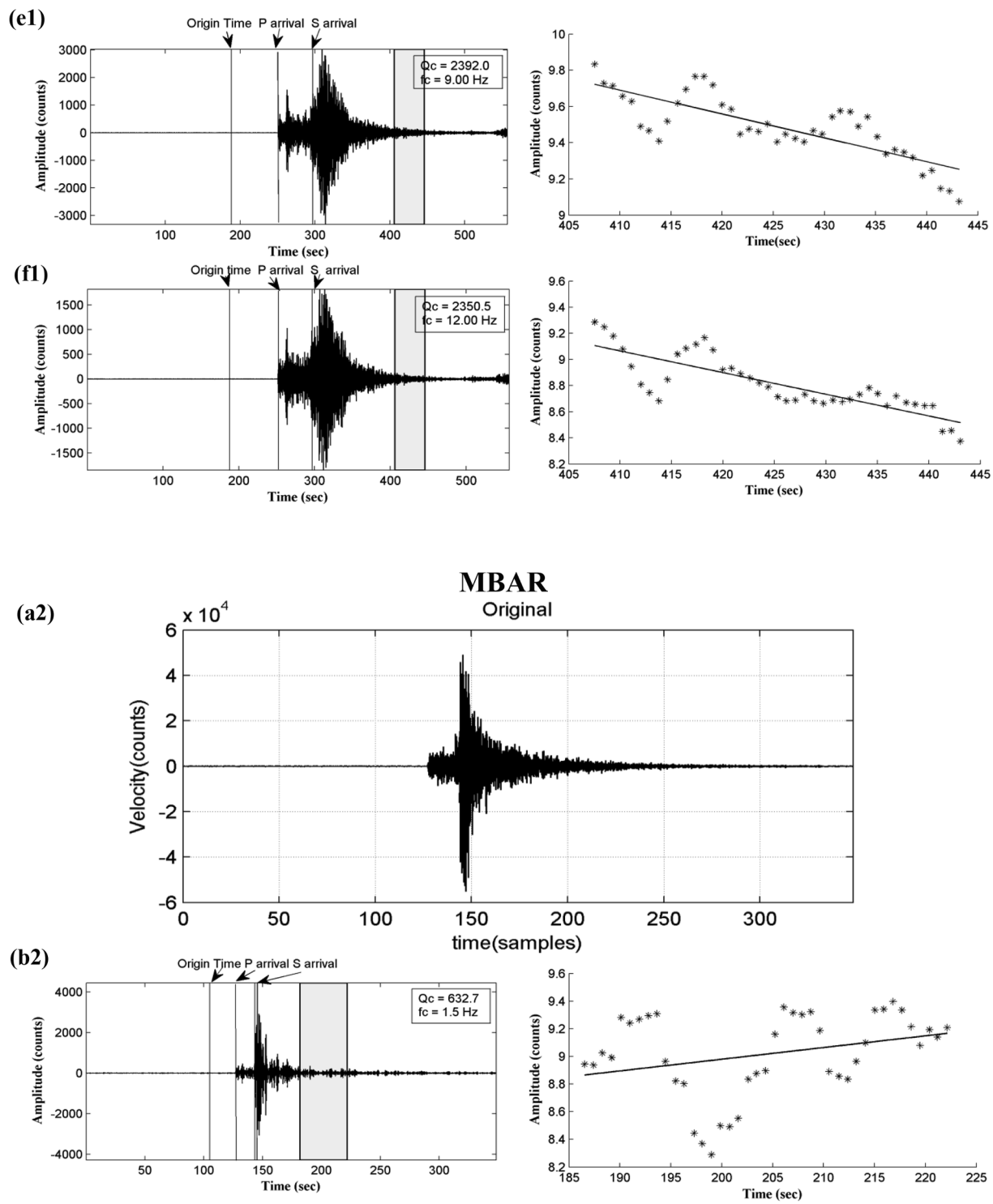


Fig. 6. (continued)

with stepping of 1 s. The natural logarithmic of root mean square (RMS) amplitude is taken and plotted as a function of lapse time t and a linear equation is fitted whose slope gives coda Q for considered central frequency (f_c). Fig. 4(b)–(f); 5(b)–(f); 6(b1)–(f3); 7(b1)–(f2) and 8(b1)–(f2) along with their corresponding original seismogram of events recorded by corresponding stations are also shown for better reliability. We used well located distant earthquakes recorded by all fifteen stations. The less number of earthquakes for the corresponding central frequency in comparison to that of other zones caused low signal-to-noise ratio. The

less number of earthquakes in analysis for the particular zone for the corresponding central frequency has a standard error and reverse is also true.

5. Results and discussion

The single backscattering model proposed by Aki and Chouet (1975) has been used to evaluate the frequency-dependent attenuation characteristic of the coda waves in the Indian Ocean region using vertical

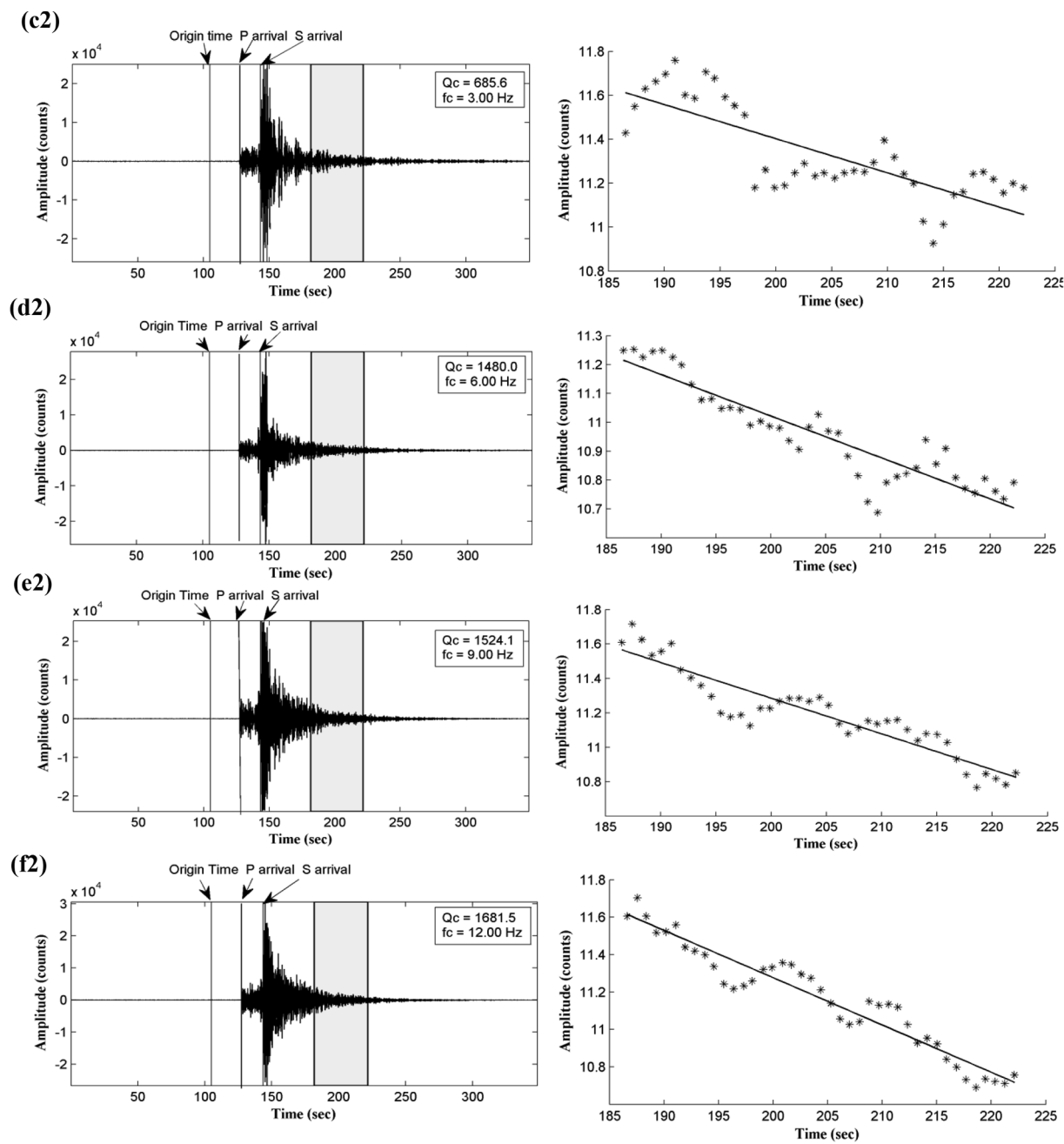


Fig. 6. (continued)

(Z) component. The seismograms have been filtered at five different bands using a Butterworth bandpass filter (Table 4). For each recording site, the frequency-dependent Q_c relation as well as average relations for the Indian Ocean province have been appraised. Estimated quality factor (Q_c) values and its comparison given with previous studies for the Indian Ocean province and analogous seismically active regions, elsewhere in the world. Our estimated attenuation characteristics along with the pertinent coda-wave quality parameter (Q_c), and frequency parameter (θ) are given in Tables 5–7.

5.1. Variation of Q_c with frequency and lapse time

The variation of estimated coda Q_c with standard errors for range of central frequencies, along with the lapse time window (LTWs) of 20, 30, 40, 50, and 60 s are listed in Tables 4 and 5. The coda Q (Q_c) values are

found to escalate with frequency and lapse time at different lapse time window (LTWs) of 20, 30, 40, 50 and 60 s. Further medium heterogeneity and the tectonic activity level in the region also has a controlled on Q_c value (e.g., Aki, 1980; Pulli and Aki, 1981; Roecker et al., 1982; Gupta et al., 1998; Vandana et al., 2015; Vandana et al., 2016). In this study, it has been found that low frequencies correspond to low- Q_c values indicates high attenuation. This is supported by high heterogeneity degree along with the decrease in the elastic strength of the rock in the ocean that is visible over the region of South of Java, Sumatra in Indonesia and Andaman Island in Indian region (Singh et al., 2012a,b; Rodriguez-Lozoya et al., 2017).

Furthermore, the lapse time dependence at all stations is categorized by an increase in Q_0 and decrease of parameter θ (Fig. 9). Q_0 has tendency to increase with lapse time that can be interpreted to increase of Q_c value due to variation in depths (Table 5). This is supported by

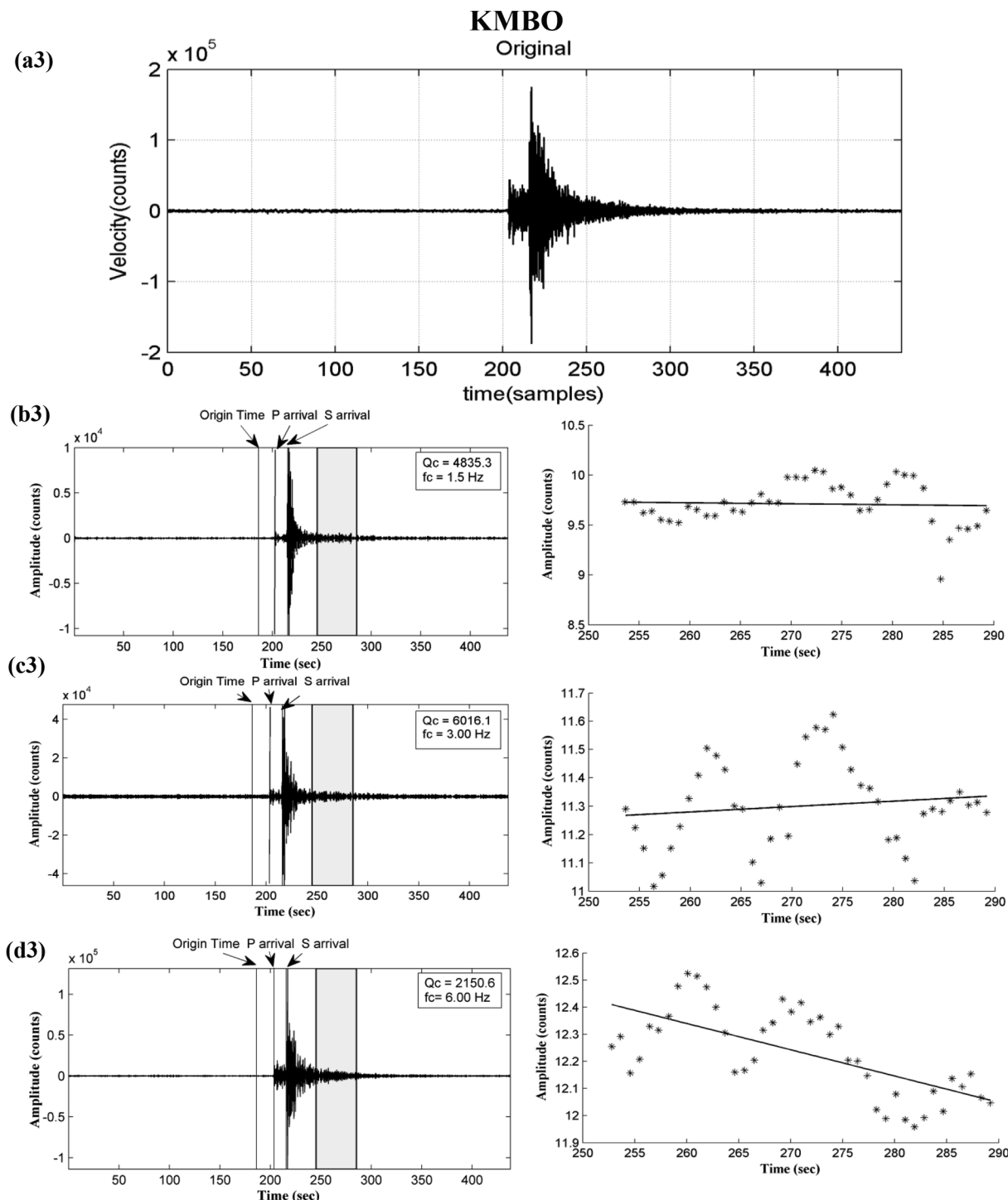


Fig. 6. (continued)

late arrival of coda wave in the seismogram that are scattered more from the deeper portion of the earth's crust and upper mantle with relatively lower attenuation than earlier energy arrival (Aki and Chouet, 1975). Strong frequency dependence behavior of Q_c in the study region is related to the degree and size of heterogeneities of the medium. The strong heterogeneity region shows significant frequency dependence of Q_c , such as subduction tectonic zones and divergent zone within the tectonically active areas (e.g., Mishra et al., 2007a,b, 2011; Padhy et al., 2011). The Q_c value increases with lapse time and that is attributed to with depth Q_c value increases. This is explained with the

consideration of longer window analysis, the larger will be the sample volume of the earth's crust and upper mantle. Similarly, with lapse time, Q_c value increases and this is explained as a function of depth by many investigators (e.g., Roecker et al. 1982; Kvamme and Havskov 1989; Ibanez et al. 1990; Woodgold 1994; Akinci et al. 1994; Gupta et al., 1998; Mukhopadhyay and Tyagi, 2007; Vandana et al., 2015). We surmise from this study that for the Indian Ocean region, increase in Q_c with larger lapse time at a given frequency, indicating the increase of Q_c value with depth. This indicates that attenuation reduces with increasing depth. According to Woodgold (1994) and Mukhopadhyay and

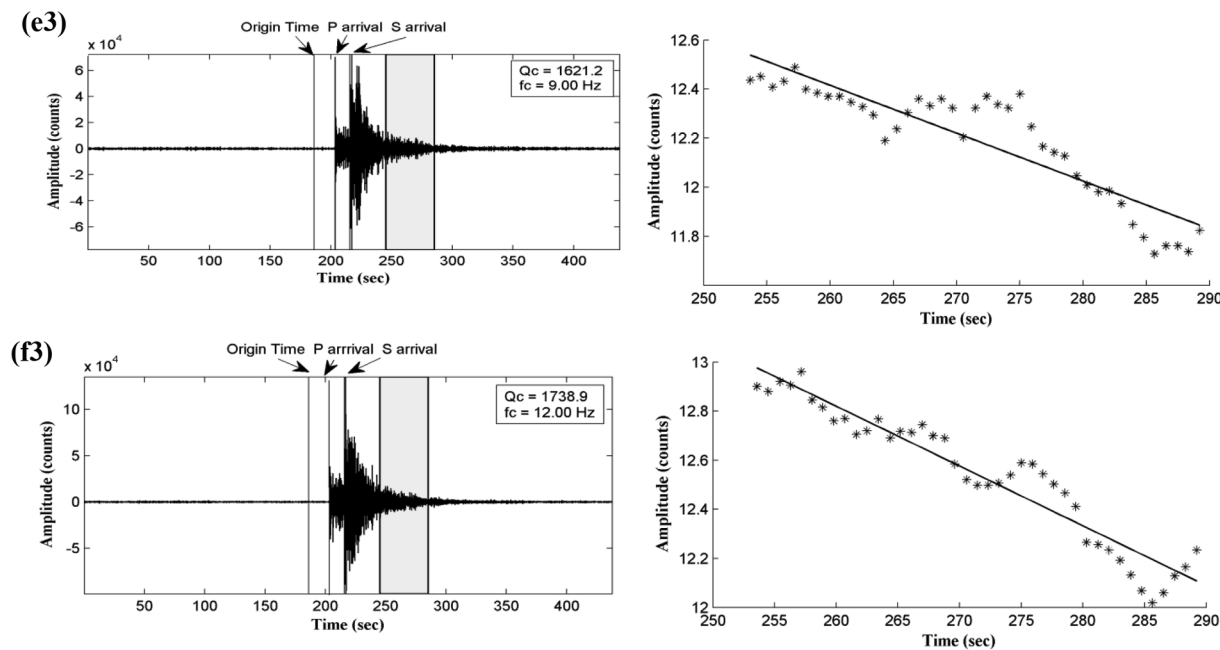


Fig. 6. (continued)

Tyagi (2007) with lapse time, the increase of Q_c value can be produced by numerous factors, which could be due to non-zero source-receiver distance with non-isotropic scattering or application of a 2-D model in place of a 3-D model or due to single scattering model where multiple scattering is prominent. In this study, the initial time of all five lapse time windows has been considered as twice of the S-wave travel time (Rautian and Khalturin 1978; Mukhopadhyay and Tyagi, 2007; Mohamed et al., 2010) to evade all direct waves (Aki and Chouet 1975) and curtail the effect of the first assumption.

5.2. Variations of Q_0 and frequency parameter

Numerous measurements have been made for change in the degree of frequency control (θ) with growing lapse time window lengths. A good relationship exist between the degree of frequency control of Q_c and the tectonic activity level in the province of estimation has been attempted by several authors for diverse tectonically active regions of the world (e.g., Aki, 1980; Pulli and Aki, 1981; Roecker et al., 1982; Pulli, 1984; Eck, 1988; Akinci et al., 1994; Gupta et al., 1998). The higher θ value ($\theta = 1.11$ at 20 s lapse time) indicates for tectonically active regions (Table 6) in which prevalence of complex faulting or subduction processes might have likely to cause strong heterogeneity. In the present study, ' θ ' value significantly varies from 1.11 to 0.85 at the 20 and 60 s lapse time window length. From this, it can be deduced that the scattering and absorptions effect play dominant role for the degree of frequency dependence (θ), which shows a decreasing trend with depth for the depth range 4–692 km. This may be due to weaker heterogeneities of the sub-surface layers with depth beneath the Indian Ocean, while Q_0 value (Q_c at 1 Hz) upsurges in the province, with the lapse time from 92 to 344. This value of Q_0 and θ shows a characteristic of zones of high tectonic activity (Fig. 9). The increase of frequency parameter θ with intensity of tectonic activity characterizes the medium in the region (Aki, 1981).

Our estimates of Q_c values help to distinguish the seismicity pattern and tectonic activity of the region because seismic waves are attenuated faster in seismically active areas. It is, therefore, the less amount of quality factor (Q) reveals that seismic waves are damped at faster pace, and accordingly the region is designated as tectonically unstable (Sedaghati and Pezeshk, 2016). In general, an area characterized as

active region with $Q < 200$, and an area characterized as stable region with $Q > 600$ (Mitchell, 1995; Sato and Fehler, 1998; Kumar et al., 2005; Sertçelik, 2012). Previous studies based on the frequency parameters unraveled the fact that tectonically stable slabs are characterized by $\theta < 0.5$, similarly for regions with moderate tectonics indicated with $\theta = 0.3\text{--}0.8$, and finally $\theta > 0.8$ helps to infer tectonically active regions (Mak et al., 2004). Our analysis (Table 7) clearly suggests that all tectonic zones (I-V) of Indian Ocean are associated with the average value of frequency parameter (θ) greater than 0.8 that varies as $0.96 \leq \theta \leq 1.15$, suggesting that entire Indian Ocean is tectonically highly active and is attributed to the nature and extent of attenuation, which in turns dictates the varying amount of structural heterogeneity in different tectonic zones (Table 7).

5.3. Tectonic implications

The Indian Ocean province has a diverse tectonic environment, with spreading centers, subduction zone, faults, fractures, volcanism hot-spots. Several factors may lead to the comparatively higher scatter of the data points. The frequency control of attenuation in the study depicts that the upper most part of the lithosphere are largely heterogeneous especially in the brittle-ductile zone, that possibly due to the stress on tectonic slab in brittle-ductile transition (Aki, 2003). The tectonic activity in the provinces where the lithosphere is governed by heterogeneity is categorized by low Coda-Q values (Singh and Herrmann, 1983). The frequency parameter, θ trends to increase with the amount of tectonic activity (Aki, 1981).

The relatively low- Q_c is observed in zone I, II and III compared to Zone IV and Zone V. The zone I, II and III are consist of Triple point junction, Spreading Zone and Prominent faults of Indian Ocean with the attenuation relations: $Q_c = 156 \pm 32 f^{1.15 \pm 0.09}$, $Q_c = 171 \pm 55 f^{1.06 \pm 0.10}$ and $Q_c = 197 \pm 29 f^{0.99 \pm 0.05}$, respectively as shown in (Fig. 10 & Table 7). As mentioned above the study region is tectonically very complicated and associated with various intricate geological structures, such as the Owen Fracture zone, RTJ-Argo Fracture Zone, the Rodrigues Triple Point, the Arabian Sea Triple Junction, the Mauritius-Reunion region, the African-Somalia Plate boundary, the Somalia-Indian plate boundary, the Central Indian Ridge, the Mid-ocean ridge, the Carlsberg Ridge, the Ninety East Ridge, actively

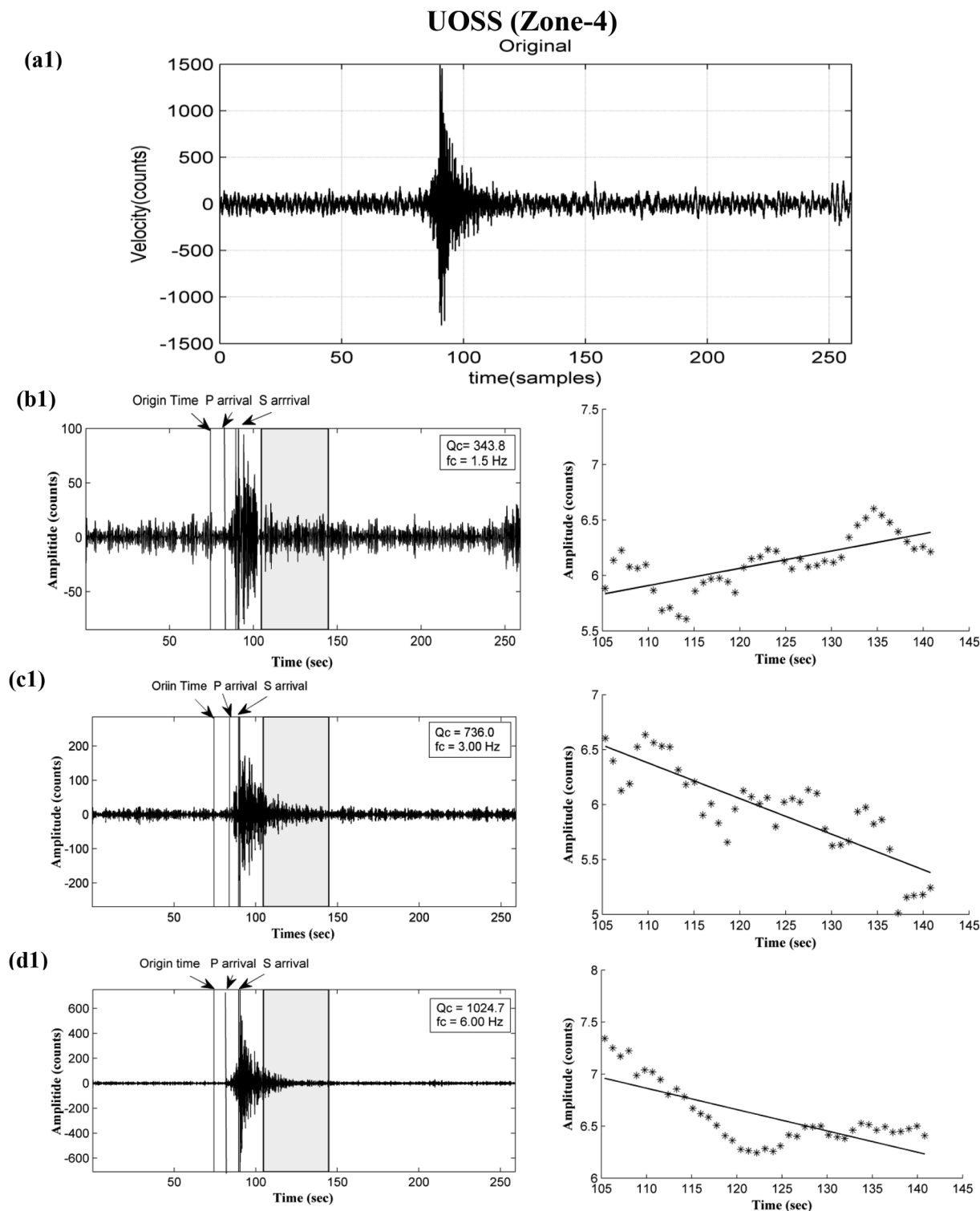


Fig. 7. (a1-a2) (Zone-4): An original plot of event of seismograms for one of the station UOSS and FURI recorded on 10-02-2014 and 18-05-2014. (b1-f2) Plot of band-pass filtered seismogram of the P, S, and coda wave portion recorded at the station with central frequency (C. F.). The best fitted linear line and estimated Q_c value for each central frequency are also shown in the figure. The coda waves portion of 40 s lapse time window length is indicated by grey window. Abbreviations P, P-wave arrival times; S, S-wave arrival time. Different zones are shown in Fig. 11.

spreading ridges, fracture and transform faults (Fig. 1) that have render the region tectonically dynamic. The greater “ θ ” (≥ 0.96) value indicates that the entire Indian Ocean is seismically more active and heterogeneous. We found that these CIR, SWIR and SEIR meet at the Rodriguez Triple Junction (RTJ) forming an inverted Y-shaped ridge

system of R-R-R (Fig. 10; Zone-I in Table 7) is associated with low- Q_c and high attenuation because of deposition of a variety of sediments at the RTJ, which is in unison to the geological mapping of the region by Souriau (1981). Zone I and II (Table 7; Fig. 10) demonstrate the existence of unidirectional discontinued ridge spreading system, causing

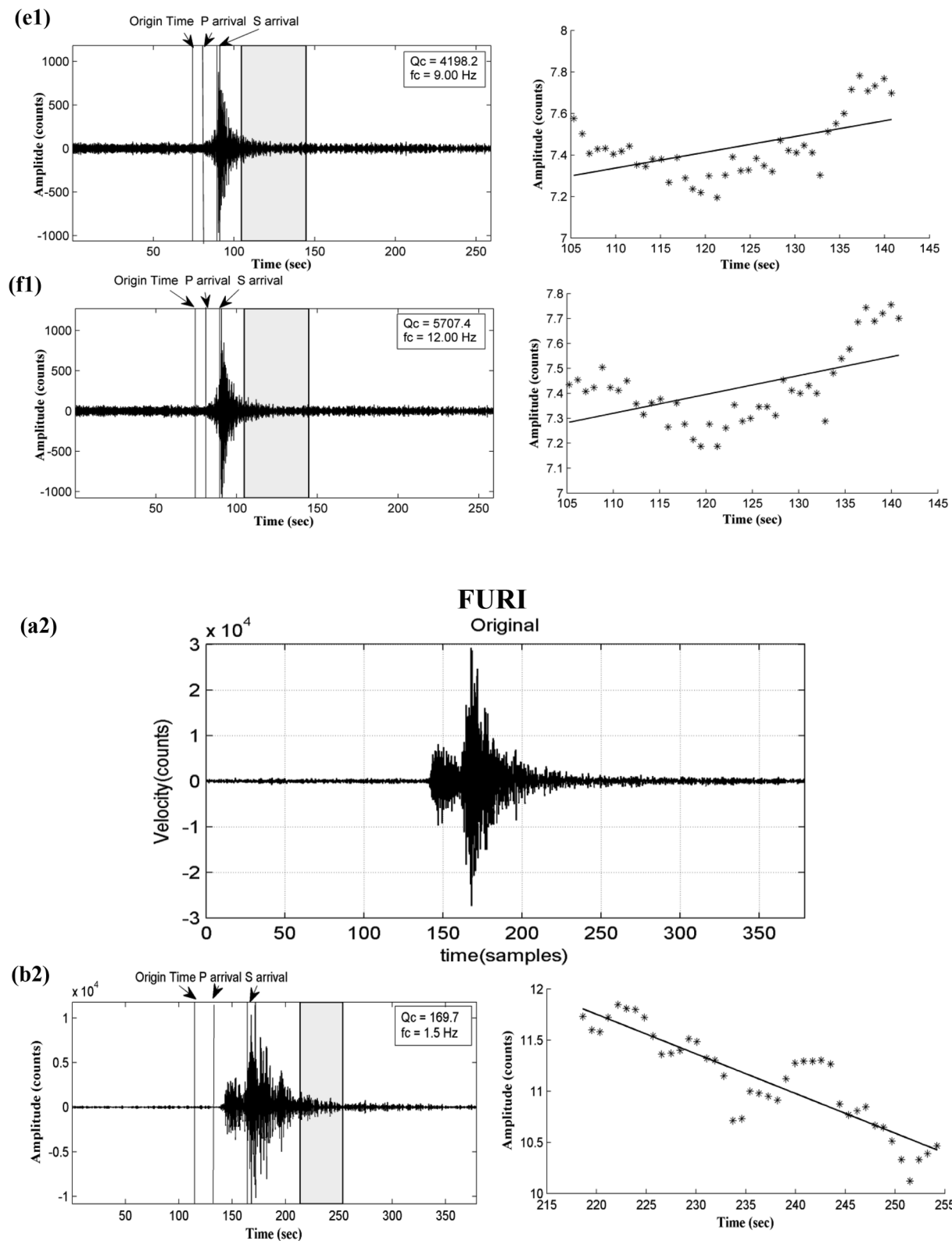


Fig. 7. (continued)

the failed rift zone having low- Q_c . Low- Q_c value of zone-I, II, III compared to that of Zone IV and V may correspond to the compressional tectonics, spreading centers and conjugate sets of faults and fracture, which in turn suggests that higher attenuation (low- Q_c) is principally caused by the seismically weaker tectonic regime whilst

active areas of fault and fracture zone of lower attenuation (highest- Q_c) may be associated with relatively competent materials in the stronger tectonic blocks beneath the Indian Ocean where shallow focus events were located in the vicinity of the subduction zones. Similar observation has also been reported for northern Cascadia subduction zone

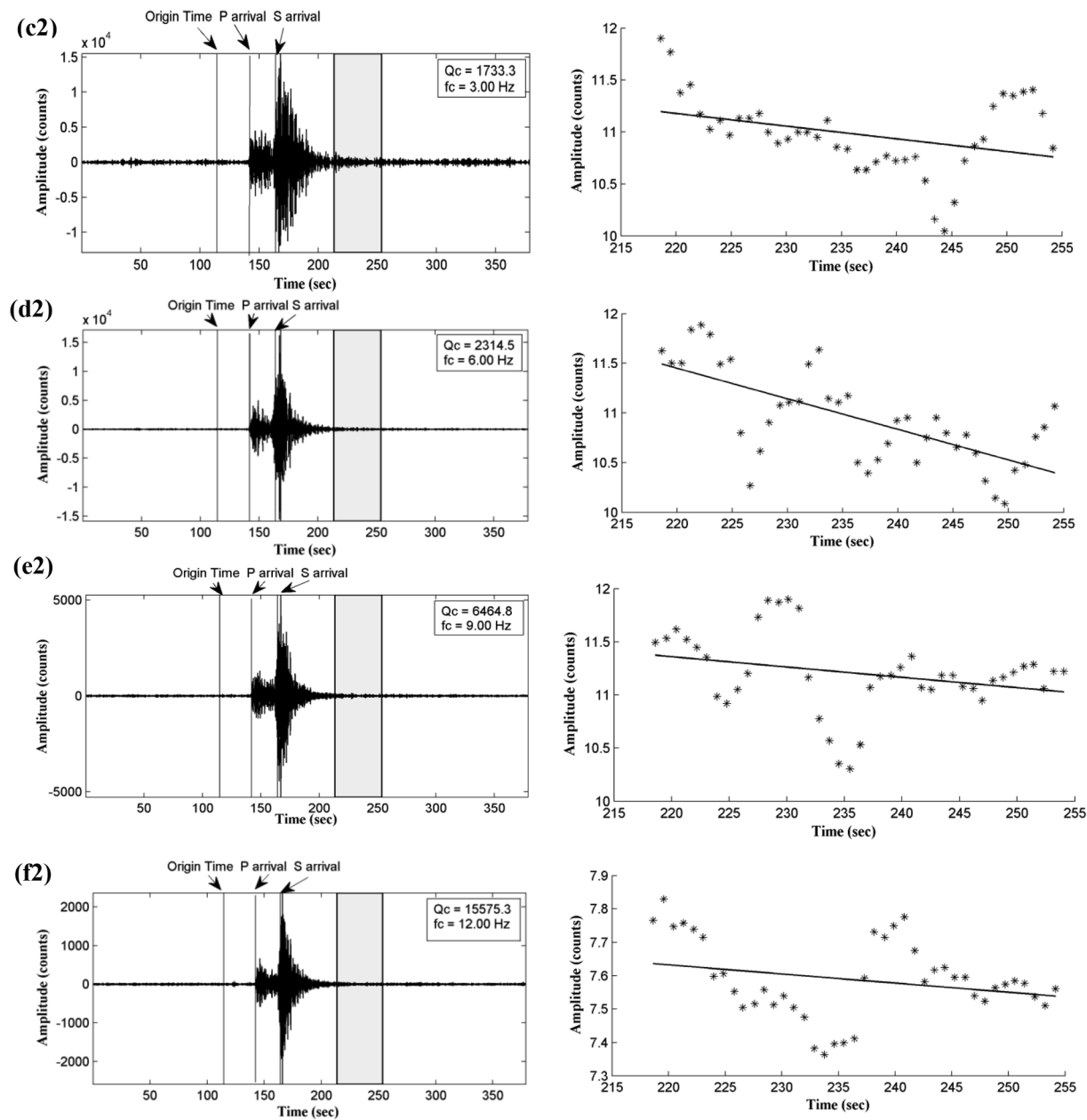


Fig. 7. (continued)

(Farahbod et al., 2016).

Most of the earthquakes are positioned along the transform faults, rather than along the spreading sections and triple junction, although there are earthquakes that are clustered at some of the ridge-transform boundaries. Here the maximum magnitude of earthquake $M_w = 8.4$ occur at fault zone having depth of 5 km having typically very low Q_c (Havskov et al., 1989). Some earthquakes are found to occur on spreading ridges, but they are inconsistent in nature, because of the comparatively high rock temperatures at the spreading centers. For the central Indian basin, along the Rodriguez triple junction, the velocity are increasing in both sides of the ridge axis, this might marked as increase in the age of the oceanic floor. These observations may be interpreted as due to the hot uprising convection current. Away from the ridge axis the material has become cooler with higher shear-wave velocity. For Ninetyeast Ridge, the shear-wave velocity of material increases with depth and reach maximum value below north of Sri Lanka, indicates the presence of cold and dense lithosphere. And also, due to

the magmatic underplating because of the crust-upper mantle transition situated at 22.5 km depth (Singh, 2005). It is pertinent to mention that the Indian Ocean is associated with thick sediment deposits, containing a variety of sediments and the fracture zones cut by numerous north-north-east trending at the Mid-Indian Ridge as observed by Souriau (1981). The materials in the Indian Ocean region are also found to be associated with elastically hard rocks (volcanic and limestone) on topographically elevated areas in the Mid-Indian Ridge where possibility of lesser attenuation can be expected whilst deep basins with abundance of manganese nodules and predominant of ilmenite placers in coastal belts can produce multi-source scattering. It is interesting to note that areas adjacent to the Indonesian Archipelago in the eastern Indian Ocean are found associated with silicic volcanic ash that may cause high degree of attenuation (low- Q_c) in the Indian Ocean. These observations are found very much corroborative with geological mapping of the region by Qasim (1999).

Across the Arabian Fan, Chagos-Lacadive Ridge, Carlsberg ridge, the

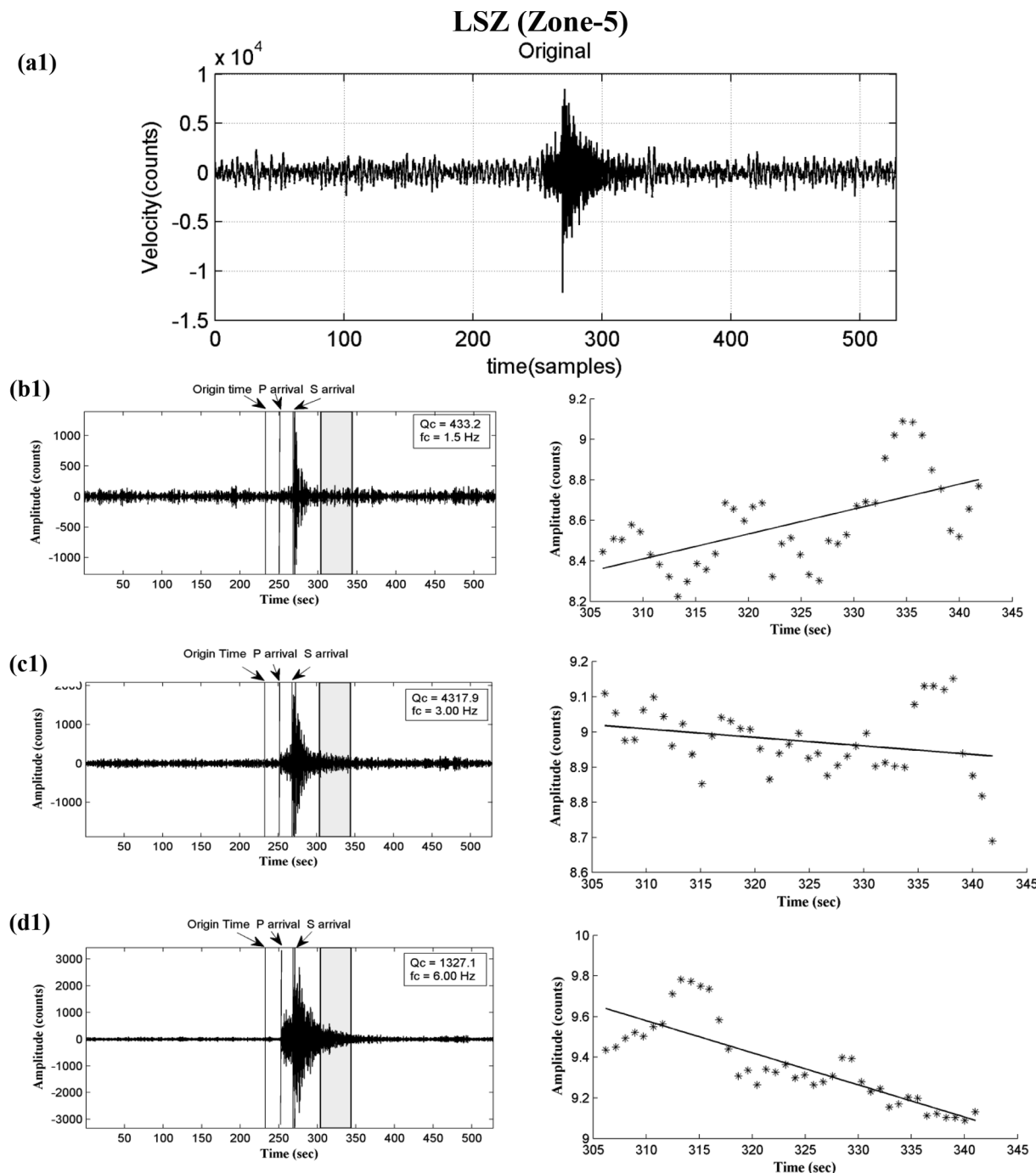
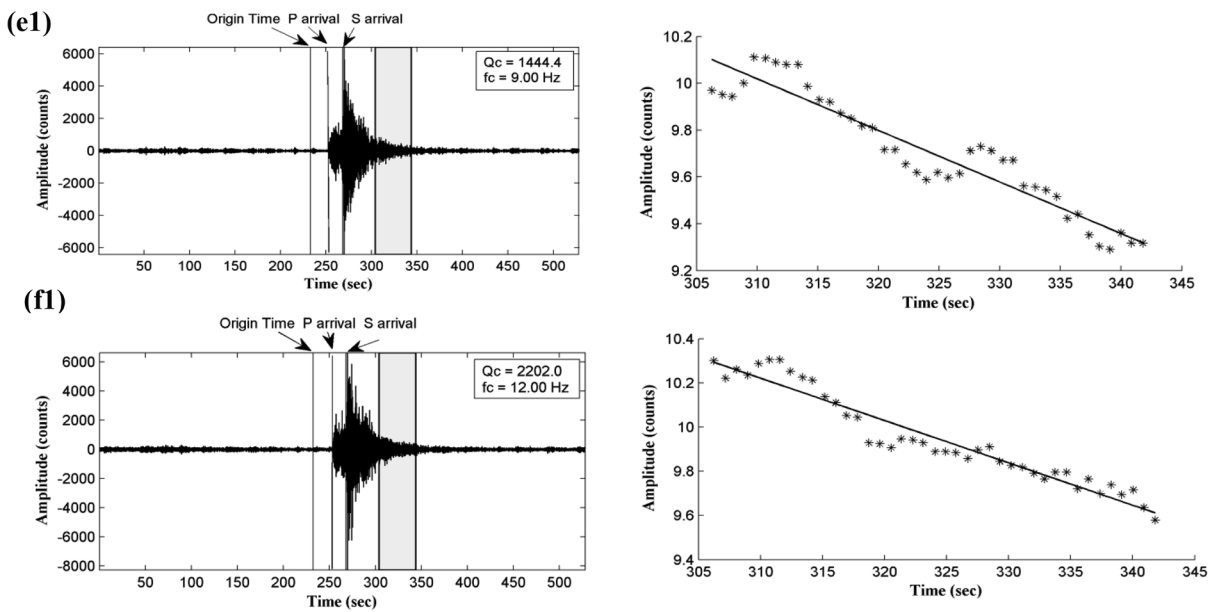


Fig. 8. (a1–a2) (Zone-5): An original plot of event of seismograms for one of the station LSZ and ABPO recorded on 26-06-14 and 19-06-2014. (b1–f2) Plot of band-pass filtered seismogram of the P, S, and coda wave portion recorded at the station with central frequency (C. F.). The best fitted linear line and estimated Q_c value for each central frequency are also shown in the figure. The coda waves portion of 40 s lapse time window length is indicated by grey window. Abbreviations P, P-wave arrival times; S, S-wave arrival time. Different zones are shown in Fig. 11.

Bay Bengal, the Ninety-east Ridge, 85°E, Central Indian Ridge (CIR), the Southeast Indian Ridge (SEIR), and the Mid-Indian Ocean (MIO) found to be associated with varying value of coda attenuation (Table 7) in which attenuation increases with depth because of increase of temperature with depth (Singh, 1990). It is well documented fact that in the vicinity of ridge there is a large sedimentary column associated with the horizontal stress increases hydrostatic pressure, which gives rise to adiabatic heating to an increase in temperature at higher depth (Singh, 1990). This observation has got support from the relatively thin lithosphere along these ridges that might have caused creation of higher

temperature zone with low-velocity anomaly that exists beneath the ridge axis. Singh (1990) also found that the high attenuation zone starts at shallow depth (80 km). There is low-Q zone across the Arabian Fan centered at 60–160 km depth, across the Off- Ninetyeast Ridge centered at 100–160 km depth and across the Ninetyeast Ridge centered at 80–160 km depth underneath the Indian Ocean province (Singh 1988). The surface wave attenuation coefficient values result the occurrence of non-homogeneities in the crust and upper-mantle underneath the Indian Ocean.

The fault and fracture zone is known to be a broad zone of



ABPO

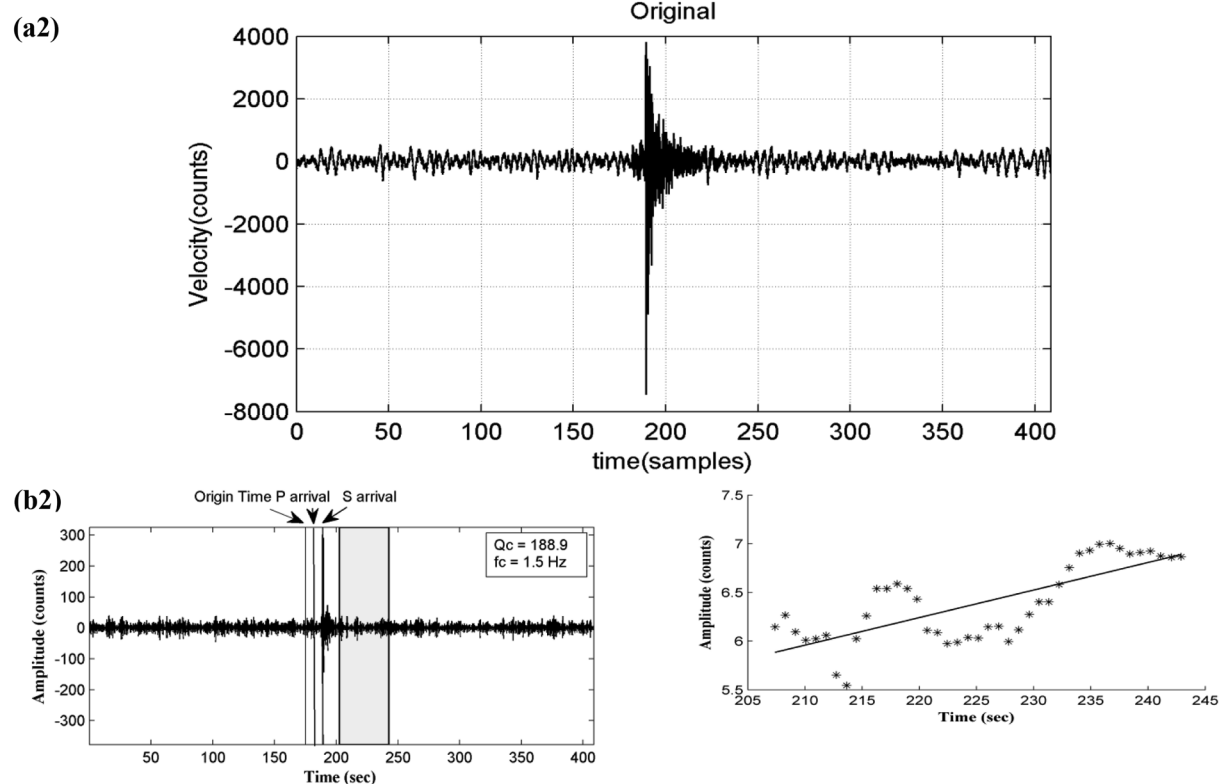


Fig. 8. (continued)

fracturing such as the West Andaman Fault (a), the Sumatran fault (b), the Sagging Fault through the Andaman-Nicobar ridge (c), Owen Fracture Zone (d), RTJ-Argo Fracture Zone (e) (Zone III, Table 7). It is, therefore, the low Q_0 here likely reflects the large sampled volume of highly fractured oceanic lithosphere, as the deformed accreted terrace along the west Sumatra/sagging fault. The lowest Q_0 values were obtained in the western part of the Indian Ocean, whereas the highest Q_0

values for the region were observed for the subduction zone.

The zone IV is found associated with volcanic and Hotspot with its attenuation relation ($Q_c = 209 \pm 39 f^{0.97 \pm 0.07}$). Most of volcanoes, such as, Afanasy Nikitin, Barren and Narcondum, the Chagos-Laccadive Ridge, Reunion hotspot are located along the ridges and subduction zone. Previous studies by Tsuru et al. (2017) showed remarkably high seismic attenuation with low- Q_0 around the volcanic and hotspot

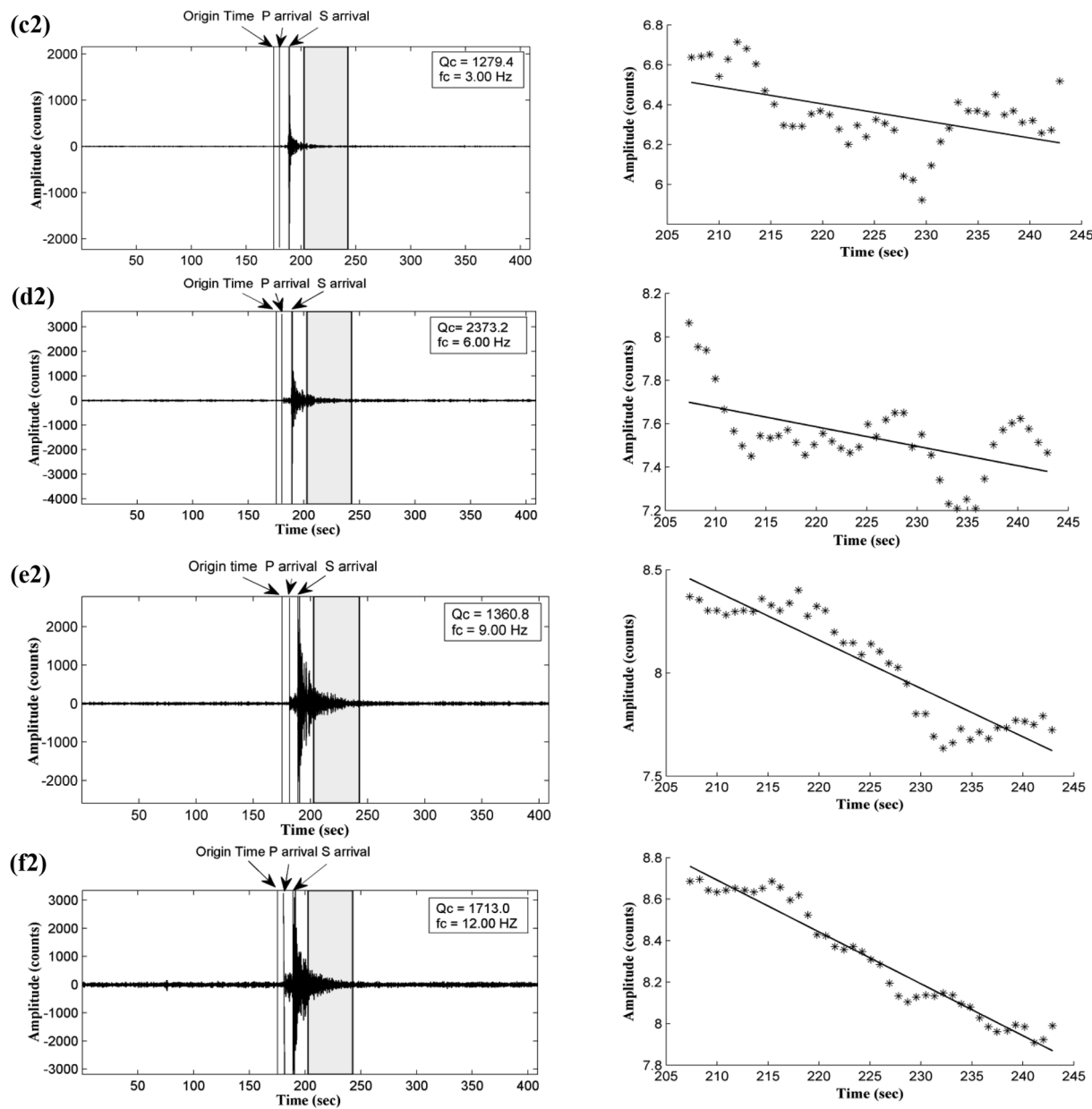


Fig. 8. (continued)

region. The high-attenuation zone is associated with fractured zone that might have generated by magma activity responsible for the genesis of moderate earthquakes (Tsuru et al., 2017). Low- Q_c shows that the region has strong regional variations in the heterogeneity of the crust due to presence of cracks, faults, and neotectonic structures (Mishra and Zhao, 2003; Singh et al., 2013; Mishra et al., 2014). The low velocity zone identified below the volcanic and hotspot region may be related to the zone of high attenuation measured from coda waves in this study, which is corroborative with earlier study made by Wu and Aki (1985). The zone of high attenuation may be ascribed to magma accumulation that contains viscous fluid, molten bodies, cracks and pores. Variations in Q_c reflect changes in the interior of the volcano that may be directly related to the magma and rock composition (Novelo-Casanova and Martínez-Bringas, 2005). The flow of magma beneath the active volcanoes (e.g., Afanasy Nikitin; the Chagos-Laccadive ridge; the Reunion Hotspot) relieves the strain that piles up along the flanks of these volcanoes.

The average attenuation relation for the subduction zone under

Zone-V, we got $Q_c = 220 \pm 33f^{0.96 \pm 0.05}$. The zone V is represented by the Northern Sumatra and The Andaman-Nicobar region, which showed low attenuation and high velocity anomalies. The low seismicity in this zone might be due to tearing of the subducting plate below this zone (Mishra et al., 2011). At very low seismicity, a remarkable creep in seismogenic block at shallow depths can be related to the lack of seismicity at deeper depths. A series of geophysical evidences such as heat flow data, Bouguer gravity anomalies, magnetic anomalies, local seismicity, and high-resolution bathymetric surveys supports our interpretation of low- Q_c in the study region. The region (subduction zone) is characterized by anomalously high heat flow (99 mW/m^2), which might have caused low- Q in the area (Curry et al., 1982; Satyavani et al., 2008). The observed high attenuation in the study area might be related to the tectonics that is attributed to the oblique convergence of the Indian plate along the Andaman trench. The Indian plate has steeply dipping subducting plate beneath the Burma micro-plate, part of the larger Sunda plate, which constitutes an ocean-continent convergent boundary (Zone V, Table 7). This fault lies below the south-west part of

Table 5

Mean value of Q_c with standard error (stderr) at each lapse time window length and at different frequency for all stations. N is the total number of observations made for each central frequency.

Stations	1.5 Hz		3.00 Hz		6.00 Hz		9.00 Hz		12.00 Hz	
	Mean \pm stderr	N	Mean \pm Stderr	N	Mean \pm Stderr	N	Mean \pm Stderr	N	Mean \pm Stderr	N
20 s										
ABPO	103.42 \pm 4	1	234.90 \pm 8.04	6	897.65 \pm 252.18	11	907.27 \pm 111.85	12	1297.83 \pm 264.85	9
CHOTO	138.62 \pm 12.31	4	150.37	1	249.98	1	584.53	1	707.13	1
COCO	143.22 \pm 32.91	2	326.46 \pm 171.41	5	809.51 \pm 326.7	2	915.68 \pm 290.45	4	1493.32 \pm 755.18	3
DGAR	110.00 \pm 25.49	6	392.44 \pm 57.05	10	891.52 \pm 178.62	12	988.78 \pm 272.71	4	1469.00 \pm 272.20	4
FURI	85.00 \pm 7.89	44	222.51 \pm 34.25	26	413.31 \pm 70.16	28	687.32 \pm 156.02	30	1525.00 \pm 118.73	22
KAPI	175.19 \pm 31.05	4	274.54 \pm 68.87	3	515.35 \pm 135.98	5	664.96 \pm 105.04	6	1475.00 \pm 263.53	5
KMBO	151.73 \pm 18.98	19	250.33 \pm 48.35	19	657.44 \pm 85.91	29	987.25 \pm 149.09	33	1341.74 \pm 126.62	40
LBTB	143.22 \pm 9.99	21	326.46 \pm 49.37	8	809.51 \pm 97.67	5	915.68 \pm 207.27	3	1523 \pm 282.78	3
LSZ	187.17 \pm 33.83	11	265.00 \pm 64.31	10	700.11 \pm 120.75	21	752.67 \pm 88.81	18	1625 \pm 139.02	15
MBAR	192.05 \pm 13.60	15	487.01 \pm 39.46	25	910.49 \pm 89.69	36	1290.34 \pm 103.57	65	1625.157 \pm 131.32	78
NWAO	72.28 \pm 29.11	4	182.54 \pm 88.47	3	862.25 \pm 211.32	5	923.35 \pm 105.32	3	1574.42 \pm 616.70	6
PALK	171.38 \pm 18.40	12	261.20 \pm 112.33	9	807.27 \pm 272.42	4	952.16 \pm 1023.32	3	1835	1
RAYN	184.91 \pm 25.32	11	412.17 \pm 77.90	9	524.96 \pm 378.77	2	825.00 \pm 74.29	8	1525 \pm 98.75	11
SUR	161.20 \pm 27.13	6	424.78 \pm 27.13	4	776.82 \pm 546.56	3	959.76 \pm 291.69	4	1551 \pm 984.37	3
UOSS	153.2173 \pm 10.97	40	326.4612 \pm 30.04	37	809.5053 \pm 91.43	34	915.6788 \pm 70.82	20	2100 \pm 153.27	17
30 s										
ABPO	210.29 \pm 50.14	3	662.53 \pm 79.66	8	1273.07 \pm 135.85	10	1490.65 \pm 278.77	13	1844.53 \pm 365.90	12
CHOTO	217.6 6 \pm 39.16	4	236.84 \pm 2.27	2	457.10 \pm 41.54	2	631.31 \pm 151.45	2	1089.05 \pm 197.81	2
COCO	233.01 \pm 24.22	4	678.07 \pm 93.58	3	1397.06 \pm 230.88	2	1890.39 \pm 967.44	2	2400.3 \pm 342.80	4
DGAR	218.71 \pm 44.81	5	477.52 \pm 47.95	16	1001.55 \pm 105.54	14	1357.37 \pm 199.93	7	2093.68 \pm 196.75	5
FURI	169.46 \pm 11.46	39	259 \pm 50.41	16	795.28 \pm 77.15	19	1156.94 \pm 134.90	19	1768.97 \pm 126.50	16
KAPI	239.80 \pm 24.99	8	500.74 \pm 21.55	4	912.98 \pm 128.35	7	1059.97 \pm 233.59	4	2571.57 \pm 464.89	4
KMBO	311.44 \pm 19.82	14	401.84 \pm 81.45	7	847.40 \pm 143.56	16	1588.64 \pm 206.11	29	1814.85 \pm 221.11	33
LBTB	233.01 \pm 14.26	20	678.07 \pm 69.45	22	1397.06 \pm 122.66	12	1890.39 \pm 215.99	11	2400.30 \pm 184.70	12
LSZ	240.90 \pm 34.31	11	387.86 \pm 112.30	10	1121.27 \pm 198.76	12	1262.73 \pm 199.52	19	1931 \pm 135.92	18
MBAR	288.03 \pm 14.44	20	750.23 \pm 49.62	28	1680.26 \pm 136.51	46	1954.06 \pm 117.54	80	2249.13 \pm 88.53	87
NWAO	209.70 \pm 66.58	4	603.02 \pm 105.95	6	1535.35 \pm 515.24	4	1848.98 \pm 396.36	8	2273.92 \pm 489.25	7
PALK	278.93 \pm 45.60	14	645.16 \pm 66.38	8	1328.14 \pm 552.94	6	1903.53 \pm 879.78	3	2521.49	1
RAYN	208.34 \pm 33.17	7	671.47	1	1107.22 \pm 454.79	2	1391.45 \pm 466.56	8	1858.61 \pm 194.84	12
SUR	225.51 \pm 71.94	4	838.71 \pm 230.52	3	1070.22 \pm 81.14	2	1336.22 \pm 4 24.54	3	2044.18 \pm 149.24	3
UOSS	253.0104 \pm 17.15	34	678.0681 \pm 32.55	32	1397.06 \pm 71.38	37	1890.39 \pm 103.41	23	2400.29	17
40 s										
ABPO	221.12	1	810.39 \pm 98.89	6	1398.29 \pm 161.09	12	1791.06 \pm 171.65	18	2003.24 \pm 189.86	15
CHOTO	247.97	1	441.52	1	503.51	1	966.48	1	1197.07 \pm 63.38	2
COCO	342.5 \pm 32.76	3	895.79 \pm 92.96	4	1494.64 \pm 733.41	3	2198.43 \pm 349.00	4	2900.36 \pm 835.49	2
DGAR	258.82 \pm 28.11	6	527.16 \pm 68.45	15	1065.77 \pm 175.12	9	1479.65 \pm 124.67	4	2267.39 \pm 374.69	3
FURI	223.92 \pm 18.34	37	276.21 \pm 42.40	10	823.08 \pm 87.64	16	1284.18 \pm 323.40	11	1883.66 \pm 199.52	10
KAPI	298.64 \pm 196.97	2	561.08 \pm 323.60	2	1097.92 \pm 177.92	2	1836.86 \pm 62.01	3	2990.24 \pm 654.42	2
KMBO	371.51 \pm 43.13	11	483.72 \pm 62.45	12	1122.65 \pm 100.92	31	1757.79 \pm 112.59	33	2117.90 \pm 123.19	38
LBTB	342.50 \pm 14.64	21	895.79 \pm 76.17	13	1494.64 \pm 135.32	14	2198.43 \pm 214.66	12	2900.36 \pm 243.14	16
LSZ	324.53 \pm 37.95	14	439.37 \pm 76.79	8	439.37 \pm 76.79	14	1450.23 \pm 197.64	14	2091.23 \pm 353.03	16
MBAR	356.88 \pm 34.98	14	802.74 \pm 44.71	25	1676.63 \pm 141.70	52	2107.89 \pm 117.75	87	2466.29 \pm 118.90	88
NWAO	369.13	1	970.80 \pm 144.06	2	1726.19 \pm 16.93	2	2112.44 \pm 592.61	5	2567.25 \pm 561.47	5
PALK	296.93 \pm 25.10	13	741.19 \pm 74.56	8	1428.82 \pm 547.43	5	2342.74 \pm 221.54	2	2812.36	0
RAYN	261.72 \pm 43.88	8	1106.15 \pm 182.16	8	1238.88 \pm 171.92	2	1931 \pm 142.71	6	2013.94 \pm 226.32	12
SUR	288.57 \pm 35.97	3	977.62 \pm 143.12	4	1141.36 \pm 132.76	2	1470.26 \pm 230.45	8	2218 \pm 660.48	7
UOSS	342.4973 \pm 16.17	29	895.795 \pm 47.54	36	1494.642 \pm 89.59	27	2198.426 \pm 213.89	18	2775 \pm 236.91	16
50 s										
ABPO	350.79	1	935.49 \pm 128.82	3	1502.11 \pm 204.59	9	1967.09 \pm 251.56	15	2225.06 \pm 292.48	12
CHOTO	274.32 \pm 21.56	2	523.32	0	626.98	1	1024.22 \pm 1717.00	2	1279.93	1
COCO	377.92 \pm 92.22	3	1086.21 \pm 48.15	4	1619.13 \pm 204.69	3	2483.25 \pm 351.96	5	2816.38 \pm 1168.01	3
DGAR	302.35 \pm 26.60	9	566.41 \pm 58.09	17	1114.67 \pm 54.38	6	1672.40 \pm 1326.33	3	2534.68	1
FURI	246.90 \pm 26.29	24	442.66 \pm 194.65	6	1062.01 \pm 304.31	10	1347.76 \pm 200.19	10	1949.99 \pm 221.66	10
KAPI	428.96 \pm 43.79	5	659.24 \pm 142.42	2	1329.40 \pm 241.58	3	1841.50 \pm 471.09	2	3713.739 \pm 1000.0	1
KMBO	357.62 \pm 57.26	10	733.08 \pm 98.38	12	1250.59 \pm 114.74	26	1932.83 \pm 196.91	29	2264.33 \pm 138.60	33
LBTB	377.92 \pm 29.47	21	1086.21 \pm 111.07	18	1619.13 \pm 126	23	2483.25 \pm 270.98	22	2816.38 \pm 199.49	23
LSZ	410.64 \pm 46.03	11	676.88 \pm 103.28	6	1255.01 \pm 236.97	9	1526.91 \pm 154.66	9	2298.51 \pm 330.27	15
MBAR	423.85 \pm 38.11	12	858.78 \pm 53.42	27	1792.65 \pm 165.62	43	2165.91 \pm 116.19	79	2744.23 \pm 166.92	87
NWAO	496.44 \pm 101.54	4	1018.36 \pm 363.19	4	1818.53 \pm 514.35	7	2324.05 \pm 253.92	7	3056.37 \pm 869.88	8
PALK	477.39 \pm 23.71	15	1006.27 \pm 116.94	10	1860.58 \pm 113.40	9	2811.77 \pm 1840.87	3	3035.8	1
RAYN	254.91 \pm 47.18	7	1250.82 \pm 142.44	4	1514.74	1	2104.92 \pm 399.47	10	2185.14 \pm 270.46	15
SUR	353.73 \pm 44.37	3	1011.98 \pm 129.67	5	1359.26 \pm 357.41	3	1562.09 \pm 478.86	4	2507.41	4
UOSS	377.9224 \pm 24.28	29	1086.211 \pm 67.90	24	1619.126 \pm 116.57	24	2483.254 \pm 263.42	8	2816.383 \pm 808.59	4
60 s										
ABPO	371.65	1	1074.66 \pm 205.14	2	1688.43 \pm 243.04	10	2125.29 \pm 367.22	17	2571.30 \pm 198.43	3
CHOTO	315.01 \pm 65.45	2	655.27 \pm 26							

Table 5 (continued)

Stations	1.5 Hz		3.00 Hz		6.00 Hz		9.00 Hz		12.00 Hz	
	Mean ± stderr	N	Mean ± Stderr	N	Mean ± Stderr	N	Mean ± Stderr	N	Mean ± Stderr	N
FURI	294.77 ± 40.93	20	781.85 ± 8.41	3	1118.74 ± 175.09	7	1858.40 ± 210.91	9	2122.76 ± 189.71	7
KAPI	553.19 ± 37.67	8	701.98 ± 107.90	1	1893.57 ± 389.20	2	2246.83 ± 373.23	1	4324.93	1
KMBO	413.49 ± 58.58	8	710.11 ± 50.04	8	1668.37 ± 145.99	24	2259.04 ± 223.80	26	2557.85 ± 197.12	28
LBTB	469.79 ± 19.34	21	1033.06 ± 103.91	20	2241.38 ± 209.92	24	2500.06 ± 188.90	24	3193.23 ± 322.19	23
LSZ	457.22 ± 63.78	9	1014.18 ± 158.36	6	1281.71 ± 225.12	7	1697.42 ± 238.47	9	2409.89 ± 454.29	10
MBAR	499.56 ± 40.07	13	1094.09 ± 70.69	27	1851.45 ± 149.30	42	2507.34 ± 161.24	76	3010.58 ± 203.13	83
NWAO	510.31 ± 118.80	3	1128.64 ± 177.68	6	2073.05 ± 147.74	5	2526.64 ± 725.08	9	3168.30 ± 516.11	8
PALK	564.54 ± 38.11	17	1264.25 ± 141.40	11	2538.23 ± 448.87	7	3029.03 ± 2415.12	2	3398.22	1
RAYN	542.15 ± 53.45	4	1289.85 ± 112.80	11	1526.87 ± 473.76	4	2082.11 ± 330.49	11	2391.63 ± 290.54	20
SUR	394.04 ± 88.23	4	1221.79 ± 286.24	5	1744.25 ± 464.89	6	2031.58 ± 126.86	3	2592.37 ± 317.41	3
UOSS	469.7853 ± 22.54	30	1033.058 ± 65.54	24	2241.38 ± 145.77	25	2500.056 ± 266.77	8	3193.23 ± 405.75	7

Table 6

Average attenuation relations for five lapse time windows obtained from the mean values of Q_c for Indian Ocean region.

Lapse time (s)	Empirical relationship
20	$Q_c = 92.04 \pm 35.07f^{1.105 \pm 0.24}$
30	$Q_c = 165.99 \pm 52.44f^{1.02 \pm 0.14}$
40	$Q_c = 220.31 \pm 58.68f^{0.96 \pm 0.10}$
50	$Q_c = 277.17 \pm 73.09f^{0.90 \pm 0.90}$
60	$Q_c = 344.99 \pm 94.98f^{0.85 \pm 0.85}$

Sumatra and the Andaman Islands. The major strike slip faults occur in the overriding plate of the subduction zone due to regional compressional stress contributed towards the variability in Q_c . Along these zones, there are much thicker sediments between the plates. The heat and pressure make the sediments warmer and compressed that resulted in slip of fault during an earthquake in the shallowest part of the subduction zone. Additionally, the process of dehydration embrittlement through crustal weakening caused due to the dehydration of hydrous minerals in the deep-seated source zones, resulted in changes of structural heterogeneities along the subduction zone (Mishra and Zhao, 2004; Zhao, 2015) that might have played an important role for lesser- Q_c and higher attenuation in the study region because dense and water-bearing sediments or accreted materials, are one of the plausible factors that brings the brittle failure (Mishra et al., 2011).

5.4. Comparison of Q_c with global observations

The attenuation characteristics of coda wave (Q_c) for single back-scattering method are used to estimate the different geological and tectonic provinces globally. Numerous measurements have been made by the global researchers for different tectonic regions (e.g., Aki and Chouet, 1975; Sato, 1977; Roecker et al., 1982; Pulli, 1984; Jin and Aki, 1988; Gupta et al., 1998; Mak et al., 2004; Sharma et al., 2008; Mohamed et al., 2010; Singh et al., 2012; Padhy et al., 2011; Vandana et al., 2015; Dobrynina et al., 2017). Our results of Q_c for different provinces are shown in Fig. 11. The frequency-dependent average Q_c relationships obtained in our study region as, $Q_c = 92.04 \pm 35.07f^{1.105 \pm 0.24}$ (20 s), $Q_c = 165.99 \pm 52.44f^{1.02 \pm 0.14}$ (30 s), $Q_c = 220.31 \pm 58.68f^{0.96 \pm 0.10}$ (40 s), $Q_c = 277.17 \pm 73.09f^{0.90 \pm 0.90}$ (50 s), $Q_c = 344.99 \pm 94.98f^{0.85 \pm 0.85}$ (60 s). Our estimated frequency-dependent average Q_c relationship of the present study is $Q_c = (220 \pm 58.68)f^{(0.96 \pm 0.08)}$ for 40 s window length is considered as the most reliable and stable solution to ensure better comparison with other tectonic regions studied by different researchers (Fig. 11). With the greater lapse time (> 40 s), the Q_0 value of the deeper portion of the crust is found to be relatively very high since higher Q_0 value along with low θ value has a trend of rapid change in crustal properties

that may not be stable and reliable for making comparison with other tectonically active regions (Jin and Aki, 1988). We, therefore compared our Q_0 and θ values of the Indian Ocean at 40 s with that of the other region of the world (e.g., Souriau, 1981; Singh and Herrmann, 1983; Scherbaum and Kisslinger, 1985; Mak et al., 2004; Yang et al., 2007; Padhy et al., 2011; McNamara et al., 2012; Singh et al., 2012a,b; Venkatesan and Gamage, 2013; Hosseini et al., 2015; Gamage and Venkatesan, 2015; Rodriguez-Lozoya et al., 2017) as shown in Fig. 11. We observed that our estimated averaged Q_c values is found to be comparable to $Q_0 = 220 \pm 58$ and a frequency-dependence $\theta = 0.96 \pm 0.10$ for Indian Ocean (Table 6) to that of Aleutian Islands (the Adak Seismic zone) (Scherbaum and Kisslinger, 1985) at low frequency (≤ 5 Hz) and to the Philippine Sea Subduction zone (Petukhin) at higher frequency range (≥ 5 Hz) (Fig. 11), which is very much correlative to our study. From this analysis, we interpreted that the tectonic settings beneath the Indian Ocean region are more complex and formed by the intersection of different plate boundaries having major faults, fracture systems and made the region seismo-tectonically active. Low Q_0 value with large ' θ ' signifies the strong scattering effects of the comparatively compressed faulted structures of the uppermost part of the crust in the region. None-the-less, the Plate boundaries have complicated folding, and faulting on the floor of the Indian Ocean region (Paul et al., 2003) that might have contributed immensely to active seismotectonic settings and variable structural heterogeneities having distinct variability in attenuation characteristics beneath the Indian Ocean region. We infer that our assimilated attenuation model has potential to provide information on intricate seismotectonics and seismogenesis for computing earthquake source parameters, earthquake hazards, and that may be useful for assimilating seismic velocity structure beneath the Indian Ocean.

6. Conclusion

The study region is tectonically very complicated and associated with various intricate geological structures, such as the Owen Fracture zone, RTJ-Argo Fracture Zone, the Rodrigues Triple Point, the Arabian Sea Triple Junction, the Mauritius-Reunion region, the African-Somalia Plate boundary, the Somalia-Indian plate boundary, the Central Indian Ridge, the Mid-ocean ridge, the Carlsberg Ridge, the Ninety East Ridge, actively spreading ridges, fracture and transform faults that have render the region tectonically dynamic. We analyzed 300-distant earthquakes recorded by IRIS network digitally positioned around the Indian Ocean province that have been studied for varying lapse time window lengths at different frequency band with a central frequency in the range of 1.5 to 12.0 Hz to estimate coda quality factor (Q_c). The frequency-dependent average Q_c relationships obtained at various lapse time window lengths that showed increase in window length has direct correlation with Q_c and frequency parameter (θ) decreases with increasing window length, which can be interpreted as the scattering effect in the study

Table 7
Showing average attenuation relations estimated for different zones of the Indian Ocean region.

Zone	No. of Earthquake	Magnitude (M_w)	Area	Attenuation $Q_c = Q_0 f^\theta$	Q_0	θ
Triple Point Junction (Zone-I)	22	5.0–6.3	The Rodrigues Triple Point, Arabian Sea Triple Junction	$Q_c = 156 \pm 32 f^{1.15 \pm 0.09}$	156 ± 32	1.15 ± 0.09
Spreading Zone (Zone II)	58	5.0–6.8	The African-Somalia plate boundary, The Somalia-Indian plate boundary, Central Indian Ridge, Mid-ocean ridge, Carlsberg Ridge, Ninety East Ridge.	$Q_c = 171 \pm 55 f^{1.06 \pm 0.10}$	171 ± 55	1.06 ± 0.10
Prominent faults of Indian Ocean region (Zone-II)	255	5.0–8.4	The West Andaman Fault (a), The Sumatran fault(b), The Sagarraing Fault across the Andaman-Nicobar ridge (c), Owen Fracture Zone (d), RTJ-Argo Fracture Zone (e)	$Q_c = 197 \pm 29 f^{0.99 \pm 0.05}$	197 ± 29	0.99 ± 0.05
Volcanic and Hotspot (Zone-IV)	175	5.0–7.8	Afanasy Nikitin, The Chagos-Laccadive Ridge, Reunion hotspot	$Q_c = 209 \pm 39 f^{0.97 \pm 0.07}$	209 ± 39	0.97 ± 0.07
Subduction Zone (Zone-V)	202	5.0–9.6	The Sunda Arc (Sumatra and Java), The Northern Sumatra and The Andaman-Nicobar region	$Q_c = 220 \pm 33 f^{0.96 \pm 0.05}$	220 ± 33	0.96 ± 0.05

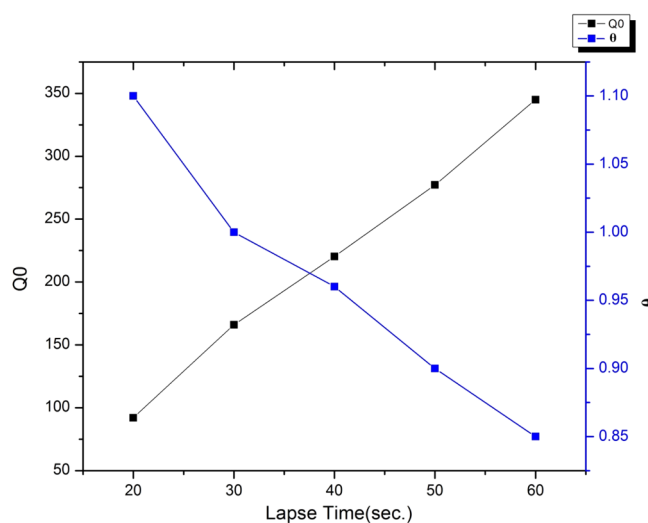


Fig. 9. Average values of " Q_0 " and " θ " as functions of lapse time.

region where increase of Q_c with increasing depth from oceanic surface is observed, which may be due to variability of structural heterogeneities at the varying depths. The relatively high value of Q_c inferred low attenuation in the oceanic floor that reveals the differential in crustal heterogeneity level within the province, reflecting extensive plate interactions and subduction and spreading effects. Our analysis clearly suggest that Indian Ocean are associated with varying frequency parameter (θ) ($0.96 \leq \theta \leq 1.15$), suggesting that entire Indian Ocean is tectonically highly active and more heterogeneous and is attributed to the nature and extent of attenuation, which in turns dictates the varying amount of structural heterogeneity in different tectonic zones. We found that these ridges, CIR, SWIR and SEIR meet at the Rodriguez Triple Junction (RTJ) forming an inverted Y-shaped ridge system of R-R is associated with low- Q_c and high attenuation because of deposition of a variety of sediments at the RTJ, which is in unison to the geological mapping of the region.

The materials in the Indian Ocean province are also found to be associated with elastically hard rocks (volcanic and limestone) on topographically elevated areas in the Mid-Indian Ridge where possibility of lesser attenuation can be expected whilst deep basins with abundance of manganese nodules and predominant of ilmenite placers in coastal belts can produce multi-source scattering. It is interesting to note that areas adjacent to the Indonesian Archipelago in the eastern Indian Ocean are found associated with silicic volcanic ash that may cause high degree of attenuation in the Indian Ocean. We observed that our estimated averaged Q_c values is found to be comparable to $Q_0 = 220 \pm 58$ and a frequency-dependence $\theta = 0.96 \pm 0.10$ for Indian Ocean to that of Aleutian Islands (the Adak Seismic zone) (Scherbaum and Kisslinger, 1985) at low frequency (≤ 5 Hz) and to the Philippine Sea Subduction zone (Petukhin) at higher frequency range (≥ 5 Hz), which is very much correlative to seismotectonic settings of these two regions. We infer that our assimilated attenuation model has potential to provide information on intricate seismotectonics and seismogenesis for computing earthquake source parameters, earthquake hazards that can be used for assimilating detailed seismic velocity structure beneath the Indian Ocean region.

Declaration of Competing Interest

The authors declare that they have no known competing financial interests or personal relationships that could have appeared to influence the work reported in this paper.

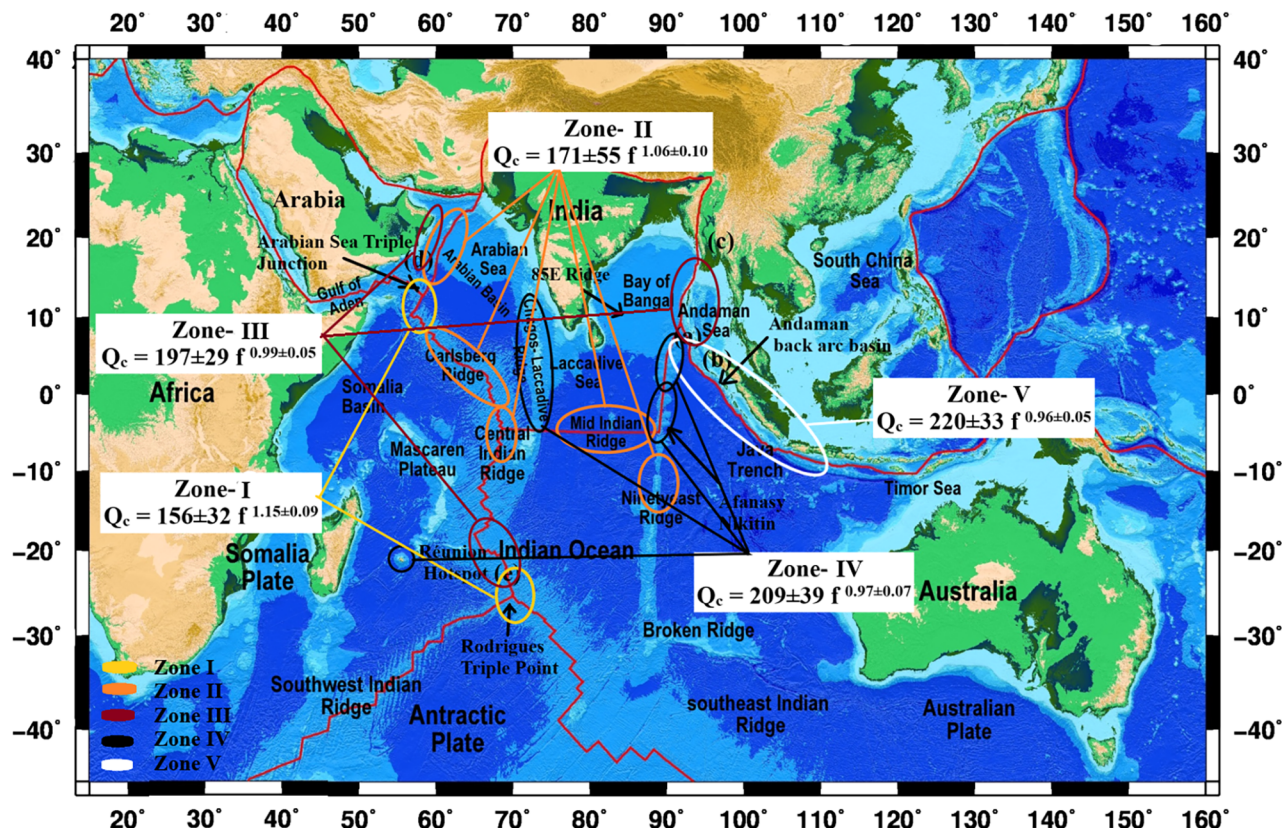


Fig. 10. Seismic attenuation zone of the study region.

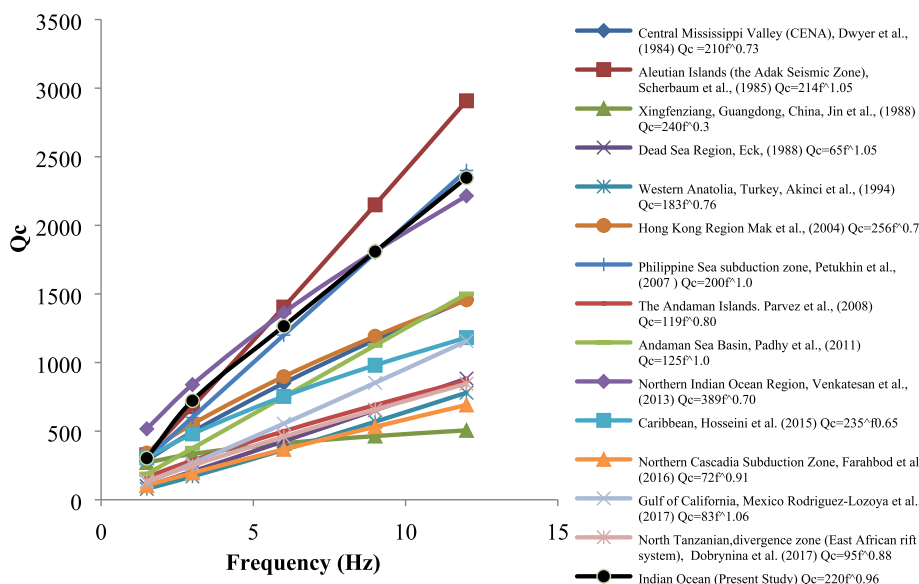


Fig. 11. Comparison of Q_c of the Indian Ocean (present study) with the other regions such as: Aleutian Islands (the Adak Seismic Zone), Scherbaum and Kisslinger (1985); Xingfenziang, Guangdong, China, Jin and Aki (1988); Dead Sea Region, Eck (1988); Western Anatolia, Turkey, Akinci et al. (1994); Hong Kong Region Mak et al. (2004); Philippine Sea subduction zone, Petukhin and Kagawa (2007); The Andaman Islands, Parvez et al. (2008); Andaman Sea Basin, Padhy et al. (2011); Northern Indian Ocean, Venkatesan et al., (2013); Caribbean, Hosseini et al. (2015); Northern Cascadia Subduction Zone, Farahbod et al. (2016); Gulf of California, Mexico Rodriguez-Lozoya et al. (2017); North Tanzanian, divergence zone (East African rift system), Dobrynina et al. (2017).

Acknowledgements

Author (MSE) are grateful to the Director, National Centre for Seismology (NCS), Ministry of Earth Sciences (MoES), New Delhi for his consistent support to seek guidance from the external research supervisor (OPM). MSE is grateful to the Director, IIT (ISM) and the Head, Department of Applied Geophysics for motivating environment to conduct this research. MSE acknowledges sincere thanks to S. K. Pal, Associate professor of Applied Geophysics, IIT(ISM) Dhanbad for fruitful discussion and feedbacks. PNSR and MSE acknowledges

Ministry of Earth Sciences, Govt. of India for partly sponsoring this work with facility (No. MOES/P.O.(Seismo)/1(148)/2012). We prepared most of figures using the GMT package (Wessel and Smith, 1998). Authors are thankful to the Incorporated Research Institutions for Seismology (IRIS) for providing data to complete this research work. The authors are grateful to the Editor, JAES and anonymous reviewers for their constructive comments and suggestions to improve the original manuscript.

Appendix A. Supplementary material

Supplementary data to this article can be found online at <https://doi.org/10.1016/j.jseaes.2019.104104>.

References

- Abercrombie, R.E., Antolik, M., Felzer, K., Ekstrom, G., 2001. The 1994 Java tsunami earthquake: Slip over a subducting seamount. *J. Geophys. Res.* 106 (B4), 6595–6607.
- Aki, K., 2003. Seismology of earthquake and volcanic prediction. In: Seventh Workshop on Non-Linear Dynamics and Earthquake Prediction. The Abdus Salam International Centre for Theoretical Physics, Trieste, Italy H, 4, pp. 1519–10.
- Aki, K., 1981. Source and scattering effects on the spectra of small local earthquakes. *Bull. Seismol. Soc. Am.* 71, 1687–1700.
- Aki, K., 1980. Attenuation of shear-waves in the lithosphere for frequencies from 0.05 to 25 Hz. *Phys. Earth Planet. Inter.* 21, 50–60.
- Aki, K., 1969. Analysis of the seismic coda of local earthquakes as scattered waves. *J. Geophys. Res.* 74, 615–631.
- Aki, K., Chouet, B., 1975. Origin of coda waves: source, attenuation, and scattering effects. *J. Geophys. Res.* 80, 3322–3342.
- Aki, K., 1996. Scale dependence in earthquake phenomena and its relevance to earthquake prediction. *Proc. Natl. Acad. Sci.* 93 (9), 3740–3747.
- Akinci, A., Eyyidoğan, H., 1996. Frequency-dependent attenuation of S and coda waves in Erzincan region (Turkey). *Phys. Earth Planet. Inter.* 97 (1–4), 109–119.
- Akinci, A., Taktak, A.G., Ergintav, S., 1994. Attenuation of coda waves in Western Anatolia. *Phys. Earth Planet. Inter.* 87, 155–165.
- Akyol, N., 2015. Lapse time dependence of coda wave attenuation in Central West Turkey. *Tectonophysics* 659, 53–62.
- Atkinson, G.M., Boore, D.M., 1995. Ground-motion relations for eastern North America. *Bull. Seismol. Soc. Am.* 85, 17–30.
- Biescas, B., Rivera, Z., Zapata, J.A., 2007. Seismic attenuation of coda waves in the eastern region of Cuba. *Tectonophysics* 429, 99–109.
- Bilek, S.L., Engdahl, E.R., 2007. Rupture characterization and aftershock relocations for the 1994 and 2006 tsunami earthquakes in the Java subduction zone. *Geophys. Res. Lett.* 34 (20).
- Bilham, R., Wallace, K., 2005. Future Mw > 8 earthquakes in the Himalaya: implications from the 26 Dec 2004 Mw = 9.0 earthquake on India's eastern plate margin. *Geol. Surv. India Spec. Publ.* 85, 1–14.
- Boulanour, A., El Moudni, L., Harnafi, M., Cherkaoui, T.E., Rahmouni, A., Boukalouch, M., Sebbani, J., 2013. Spatial variation of coda wave attenuation using aftershocks of the Al Hoceima earthquake of 24 February, 2004, Morocco. *Nat. Sci.* 5 (08), 72.
- Campillo, M., Plantet, J.L., Bouchon, M., 1985. Frequency-dependent attenuation in the crust beneath Central France from Lg waves: Data analysis and numerical modeling. *Bull. Seismol. Soc. Am.* 75 (5), 1395–1411.
- Curray, J.R., 2005. Tectonics and history of the Andaman Sea region. *J. Asian Earth Sci.* 25, 187–232.
- Curray, J.R., Emmel, F.J., Moore, D.G., Raitt, R.W., 1982. Structure, tectonics, and geological history of the northeastern Indian Ocean. *The Ocean Basins and Margins. Springer* 399–450.
- Curray, J.R., Moore, D.G., Lawver, L.A., Emmel, F.J., Raitt, R.W., Henry, M., Kieckhefer, R., 1979. Tectonics of the Andaman Sea and Burma: convergent margins.
- Das, R., Mukhopadhyay, S., Singh, R.K., Baidya, P.R., 2018. Lapse time and frequency-dependent coda wave attenuation for Delhi and its surrounding regions. *Tectonophysics* 738, 51–63.
- Demopoulos, A.W.J., Smith, C.R., Tyler, P.A., 2014. The deep Indian Ocean region floor article 2014 (Chapter 7).
- Dewey, J.F., 2007. The secular evolution of plate tectonics and the continental crust: an outline. *MEMOIRS-Geo. Soc. Am.* 200, 1.
- Dobrynina, A.A., Albaric, A., Deschamps, A., Perrot, J., Ferdinand, R.W., Deverchere, J., Sankov, V.A., Chechelnitskii, V.V., 2017. Seismic wave attenuation in the lithosphere of the North Tanzanian divergence zone (East African rift system). *Russ. Geo. Geophys.* 58 (2), 253–265.
- Dobrynina, A.A., 2011. Coda-wave attenuation in the Baikal rift system lithosphere. *Phys. Earth Planet. Inter.* 188, 121–126.
- Dwyer, D.J., Herrmann, R.B., Nutti, O.W., 1984. Use of a digital seismic network to study Lg attenuation and the coda Q in the Central Mississippi Valley. *Earthquake Notes* 55 (3), 7–8.
- van Eck, T., 1988. Attenuation of coda waves in the Dead Sea region. *Bull. Seismol. Soc. Am.* 78, 770–779.
- Fitch, T.J., 1970. Earthquake mechanisms in the Himalayan, Burmese, and Andaman regions and continental tectonics in central Asia. *J. Geophys. Res.* 75, 2699–2709.
- Farahbod, A.M., Calvert, A.J., Cassidy, J.F., Brillon, C., 2016. Coda Q in the northern Cascadia subduction zone. *Bull. Seismol. Soc. Am.* 106, 1939–1947.
- Gamage, P., Venkatesan, S., 2015. Attenuation and apparent source characteristics in the northern Indian oceanic crust surrounding Sri Lanka. *Bull. Seismol. Soc. Am.* 105 (4), 2041–2057.
- Gao, L.S., Biswas, N.N., Lee, L.C., Aki, K., 1983a. Effects of multiple scattering on coda waves in three-dimensional medium. *Pure Appl. Geophys.* 121, 3–15.
- Gao, L.S., Lee, L.C., Biswas, N.N., Aki, K., 1983b. Comparison of the effects between single and multiple scattering on coda waves for local earthquakes. *Bull. Seismol. Soc. Am.* 73, 377–389.
- Gholamzadeh, A., Rahimi, H., Yaminifard, F., 2013. Spatial and temporal variation of coda-wave attenuation in the Faryab region, southeast of the Sanandaj-Sirjan zone, using aftershocks of the Tiab earthquake of 28 February 2006. *Bull. Seismol. Soc. Am.* 104 (1), 529–539.
- Guo, M.-Q., Fu, L.-Y., Ba, J., 2009. Comparison of stress-associated coda attenuation and intrinsic attenuation from ultrasonic measurements. *Geophys. J. Int.* 178, 447–456.
- Gupta, A.K., Sutar, A.K., Chopra, S., Kumar, S., Rastogi, B.K., 2012. Attenuation characteristics of coda waves in Mainland Gujarat (India). *Tectonophysics* 530, 264–271.
- Gupta, S.C., Teotia, S.S., Rai, S.S., Gautam, N., 1998. Coda Q estimates in the Koyna region, India. In: *Q of the Earth: Global, Regional, and Laboratory Studies*. Springer, pp. 713–731.
- Haldar, D., 1992. Volcanic eruption of the Barren island volcano, Andaman Sea. *J. Geol. Soc. India* 39 (5), 411–419.
- Hamilton, W.B., 1979. Tectonics of the Indonesian region. 1078. US Govt. Print. Off.
- Hasegawa, H.S., 1985. Attenuation of Lg waves in the Canadian Shield. *Bull. Seismol. Soc. Am.* 75, 1569–1582.
- Havskov, J., Malone, S., McClurg, D., Crosson, R., 1989. Coda Q for the state of Washington. *Bull. Seismol. Soc. Am.* 79, 1024–1038.
- Havskov, J., Ottemoller, L., 2003. SEISAN: the earthquake analysis software for Windows. Solaris, Linux, Mac OSX Version 8, 244.
- Herrmann, R.B., 1980. Q estimates using the coda of local earthquake. *Bull. Seismol. Soc. Am.* 70, 447–468.
- Hosseini, M., Pezeshk, S., Haji-Soltani, A., Chapman, M., 2015. Investigation of attenuation of the Lg-wave amplitude in the Caribbean region. *Bull. Seismol. Soc. Am.* 105, 734–744.
- Ibanez, J.M., Del Pezzo, E., De Miguel, F., Herraiz, M., Alguacil, G., Morales, J., 1990. Depth-dependent seismic attenuation in the Granada zone (Southern Spain). *Bull. Seismol. Soc. Am.* 80, 1232–1244.
- Jackson, D.D., Anderson, D.L., 1970. Physical mechanism of seismic waves attenuation. *Rev. Geophys. Space Phys.* 8, 1–63.
- Jhingran, A.G., 1952. Records of the Geological Survey Of India. 82(2), 300–307.
- Jin, A., Aki, K., 1988. Spatial and temporal correlation between coda Q and seismicity in China. *Bull. Seismol. Soc. Am.* 78, 741–769.
- Kanayev, V.F., Morgan, J.R., Verlaan, P.A., 2017. Article “Indian Ocean”. Encyclopedia Britannica, inc. <https://www.britannica.com/place/Indian-Ocean>.
- Kayal, J.R., Gaonkar, S.G., Chakraborty, G.K., Singh, O.P., 2004. Aftershocks and seismotectonic implications of the 13 September 2002 earthquake (M w 6.5) in the Andaman Sea basin. *Bull. Seismol. Soc. Am.* 94, 326–333.
- Kenji, K., Yoshinobu, T., 1995. Tsunami of the Sumba Earthquake of August 19, 1977. *J. Nat. Dis. Sci.* 17 (2), 87–100.
- Knopoff, L., 1964. Q. *Rev. Geophys.* 2 (4), 625–660.
- Kopnichenko, Y.F., 1977. The role of multiple scattering in the formation of seismogram's tail. *Izv. Akad. Nauk SSSR. Fiz. Zem.* 13, 394–398.
- Kumar, N., Mate, S., Mukhopadhyay, S., 2014. Estimation of Q_p and Q_s of Kinnair Himalaya. *J. Seismol.* 18 (1), 47–59.
- Kumar, N., Parvez, I.A., Virk, H.S., 2005. Estimation of coda wave attenuation for NW Himalayan region using local earthquakes. *Phys. Earth Planet. Inter.* 151, 243–258.
- Kumar, P., Joshi, A., Kumar, A., Chadha, R.K., 2015. Detailed attenuation study of shear waves in the Kumaon Himalaya, India, using the inversion of strong-motion data. *Bull. Seismol. Soc. Am.* 105 (4), 1836–1851.
- Kumar, S., Singh, Priyamvada, Singh, Pitam, Biswal, S., Parija, M.P., 2016. Frequency dependent attenuation characteristics of coda waves in the Northwestern Himalayan (India) region. *J. Asian Earth Sci.* 117, 337–345.
- Kumar, N., Yadav, D.N., 2019. Coda Q estimation for Kinnair region and surrounding part of NW Himalaya. *J. Seismol.* 23 (2), 271–285.
- Kvamme, L.B., Havskov, J., 1989. Q in southern Norway. *Bull. Seismol. Soc. Am.* 79, 1575–1588.
- Lay, T., Kanamori, H., Ammon, C.J., Nettles, M., Ward, S.N., Aster, R.C., Beck, S.L., Bilek, S.L., Brudzinski, M.R., Butler, R., DeShon, H.R., 2005. The great Sumatra-Andaman earthquake of 26 December 2004. *Sci.* 308 (5725), 1127–1133.
- Le Dain, A.Y., Tapponnier, P., Molnar, P., 1984. Active faulting and tectonics of Burma and surrounding regions. *J. Geophys. Res. Solid Earth* 89 (B1), 453–472.
- Lienert, B.R., Berg, E., Frazer, L.N., 1986. HYPOCENTER: an earthquake location method using centered, scaled, and adaptively damped least squares. *Bull. Seismol. Soc. Am.* 76, 771–783.
- Lienert, B.R., Havskov, J., 1995. A computer program for locating earthquakes both locally and globally. *Seismol. Res. Lett.* 66, 26–36.
- Mandal, P., Jainendra, Joshi, S., Kumar, S., Bhunia, R., Rastogi, B.K., 2004. Low coda Q_c in the epicentral region of the 2001 Bhuj earthquake of Mw 7.7. *Pure Appl. Geophys.* 161, 1635–1654.
- Mak, S., Chan, L.S., Chandler, A.M., Koo, R.C.H., 2004. Coda Q estimates in the Hong Kong region. *J. Asian Earth Sci.* 24, 127–136.
- McCloskey, J., Nalbant, S.S., Steacy, S., 2005. Indonesian earthquake: Earthquake risk from co-seismic stress. *Nature* 434 (7031), 291.
- McNamara, D., Meremonte, M., Maharry, J.Z., Mildore, S., Altidore, J.R., Anglade, D., Hough, S.E., Given, D., Benz, H., Gee, L., 2012. Frequency dependent seismic attenuation within the Hispaniola Island region of the Caribbean Sea. *Bull. Seismol. Soc. Am.* 102, 773–782.
- Mishra, O.P., Kayal, J.R., Chakraborty, G.K., Singh, O.P., Ghosh, D., 2007a. Aftershock investigation in the Andaman-Nicobar Islands of India and its seismotectonic implications. *Bull. Seismol. Soc. Am.* 97, S71–S85.
- Mishra, O.P., Chakraborty, G.K., Singh, O.P., Kayal, J.R., Ghosh, D., 2007b. Aftershock investigation in the Andaman-Nicobar Islands: an antidote to public panic. *Seismol. Res. Lett.* 78 (6), 591–600.
- Mishra, O.P., Singh, A.P., Kumar, D., Rastogi, B.K., 2014. An insight into Crack density, Saturation rate and Porosity model of the 2001 Bhuj earthquake in the Stable Continental Region of Western India. *J. of Asian Earth Sciences* 83, 48–59.
- Mishra, O.P., Zhao, D., 2003. Crack density, saturation rate and porosity at the 2001 Bhuj, India, earthquake hypocenter:a fluid-driven earthquake? *Earth Planet. Sci. Lett.* 212,

- 393–405.
- Mishra, O.P., Zhao, D., 2004. Seismic evidence for dehydration embrittlement of the subducting Pacific slab. *Geophys. Res. Lett.* 31.
- Mishra, O.P., Zhao, D., Ghosh, C., Wang, Z., Singh, O.P., Ghosh, B., Mukherjee, K.K., Saha, D.K., Chakrabortty, G.K., Gaonkar, S.G., 2011. Role of crustal heterogeneity beneath Andaman-Nicobar Islands and its implications for coastal hazard. *Nat. Hazards* 57, 51–64.
- Mishra, O.P., Zhao, D., Singh, D.D., 2005a. Surface-wave studies beneath the Pacific Ocean. *Bull. Seismol. Soc. Am.* 95, 2152–2161.
- Mishra, O.P., Zhao, D., Singh, D.D., 2005b. Northwest Pacific fundamental mode Rayleigh-wave group velocity and its relationship with tectonic structures. *Bull. Seismol. Soc. Am.* 95 (6), 2125–2135.
- Mitchell, B.J., 1995. Anelastic structure and evolution of the continental crust and upper mantle from seismic surface wave attenuation. *Rev. Geophys.* 33 (4), 441–462.
- Mohamed, H.H., Mukhopadhyay, S., Sharma, J., 2010. Attenuation of coda waves in the Aswan Reservoir area, Egypt. *Tectonophysics* 492 (1–4), 88–98.
- Mukhopadhyay, S., Tyagi, C., 2007. Lapse time and frequency-dependent attenuation characteristics of coda waves in the Northwestern Himalayas. *J. Seismol.* 11 (2), 149–158.
- Mukhopadhyay, S., Sharma, J., 2010. Attenuation characteristics of Garwhal-Kumaun Himalayas from analysis of coda of local earthquakes. *J. Seismo.* 14 (4), 693–713.
- Naghavi, M., Rahimi, H., Moradi, A., Mukhopadhyay, S., 2017. Spatial variations of seismic attenuation in the North West of Iranian plateau from analysis of coda waves. *Tectonophysics* 708, 70–80.
- Newcomb, K.R., McCann, W.R., 1987. Seismic history and seismotectonics of the Sunda Arc. *J. Geophys. Res.: Solid. Earth* 92 (B1).
- Novelo-Casanova, D.A., Martínez-Bringas, A., 2005. A seismic attenuation zone below Popocatépetl volcano inferred from coda waves of local earthquakes. *Geofísica Int.* 44, 177–186.
- Okal, E.A., Stein, S., 1987. The 1942 Southwest Indian Ocean Ridge Earthquake: Largest ever recorded on an oceanic transform. *Geophys. Res. Lett.* 14 (2), 147–150.
- Ortiz, M., Bilham, R., 2003. Source area and rupture parameters of the 31 December 1881 $M_w = 7.9$ Car Nicobar earthquake estimated from tsunamis recorded in the Bay of Bengal. *J. Geophys. Res.* 108 (B4), 2215.
- Padhy, S., Subhadra, N., Kayal, J.R., 2011. Frequency-dependent attenuation of body and coda waves in the Andaman Sea basin. *Bull. Seismol. Soc. Am.* 101, 109–125.
- Parvez, I.A., Sutar, A.K., Mridula, M., Mishra, S.K., Rai, S.S., 2008. Coda Q estimates in the Andaman Islands using local earthquakes. *Pure Appl. Geophys.* 165 (9–10), 1861–1878.
- Paul, A., Gupta, S.C., Pant, C.C., 2003. Coda Q estimates for Kumaun Himalaya. *J. Earth Syst. Sci.* 112, 569–576.
- Pujades, L.G., Ugalde, A., Canas, J.A., Navarro, M., Badal, F.J., Corchete, V., 1997. Intrinsic and scattering attenuation from observed seismic codas in the Almeria Basin (southeastern Iberian Peninsula). *Geophys. J. Int.* 129 (2), 281–291.
- Pujades, L.G., Canas, J.A., Egocue, J.J., Puigvi, M.A., Gallart, J., Lana, X., Pous, J., Casas, A., 1990. Coda-Q distribution in the Iberian Peninsula. *Geophys. J. Int.* 100, 285–301.
- Pulli, J.J., 1984. Attenuation of coda waves in New England. *Bull. Seismol. Soc. Am.* 74, 1149–1166.
- Pulli, J.J., Aki, K., 1981. Attenuation of seismic waves in the lithosphere: comparison of active and stable areas. In: Proc. Earthquake & Earthquake Eng.: The eastern U.S., pp. 129–141.
- Petukhin, A., Kagawa, T., 2007. High seismic attenuation in the reflective layers of the Philippine Sea Subduction Zone, Japan. *Geophys. Monograph-Am. Geophys. Union* 172, 117.
- Qasim, S.Z., 1999. The Indian Ocean: images and realities. Oxford and IBH Publishing Company.
- Rao, R., Seshamma, C.V., Mandal, P., 1998. Estimation of Coda Qc and spectral characteristics of some moderate earthquakes of southern Indian peninsula. Unpubl. Rep.
- Rajendran, C.P., Earnest, A., Rajendran, K., Das, R.D., Kesavan, S., 2003. The 13 September 2002 North Andaman (Diglipur) earthquake: An analysis in the context of regional seismicity. *Cur. Sci.* 84 (7).
- Rautian, T.G., Khalturin, V.I., 1978. The use of the coda for determination of the earthquake source spectrum. *Bull. Seismol. Soc. Am.* 68, 923–948.
- Rodriguez-Lozoya, H.E., Dominguez, R., Quintanar Robles, L., Aguilar Melendez, A., Rodriguez-Leyva, H.E., Plata Rocha, W., Garcia Paez, F., 2017. Attenuation of Coda Waves in the Central Region of the Gulf of California, México. *Geofísica Int.* 56, 137–145.
- Roecker, S.W., Tucker, B., King, J., Hatzfeld, D., 1982. Estimates of Q in central Asia as a function of frequency and depth using the coda of locally recorded earthquakes. *Bull. Seismol. Soc. Am.* 72, 129–149.
- Sato, H., 1977. Energy propagation including scattering effects single isotropic scattering approximation. *J. Phys. Earth* 25, 27–41.
- Sato, H., Fehler, M.C., 1998. Seismic wave propagation and scattering in the heterogeneous earth. Springer-Verlag, New York, pp. 308.
- Satyavani, N., Sain, K., Lall, M., Kumar, B.J.P., 2008. Seismic attribute study for gas hydrates in the Andaman Offshore India. *Mar. Geophys. Res.* 29, 167–175.
- Scherbaum, F., Kisslinger, C., 1985. Coda Q in the Adak seismic zone. *Bull. Seismol. Soc. Am.* 75, 615–620.
- Sedaghati, F., Pezeshk, S., 2016. Estimation of the coda- wave attenuation and geometrical spreading in the New Madrid seismic zone. *Bull. Seismol. Soc. Am.* 106, 1482–1498.
- Sertçelik, F., 2012. Estimation of coda wave attenuation in the east Anatolia fault zone, Turkey. *Pure Appl. Geophys.* 169, 1189–1204.
- Sharma, B., Gupta, A.K., Devi, D.K., Kumar, D., Teotia, S.S., Rastogi, B.K., 2008. Attenuation of high-frequency seismic waves in Kachchh Region, Gujarat, India. *Bull. Seismol. Soc. Am.* 98, 2325–2340.
- Singh, A.P., Mishra, O.P., Rastogi, B.K., Mahesh, P., 2013. Crustal heterogeneities beneath the 2011 Talala, Saurashtra earthquake, Gujarat, IndiaSource Zone:Seismological Evidence for Neo-tectonics. *J. Asian Earth Sciences* 62, 672–689.
- Singh, R., Paul, A., Kumar, A., Kumar, P., Sundriyal, Y.P., 2018. Estimation and applicability of attenuation characteristics for source parameters and scaling relations in the Garhwal Kumaun Himalaya region India. *J. Asian Earth Sci.* 59, 42–59.
- Singh, C., Basha, S.K., Shekar, M., Chadha, R.K., 2012a. Spatial variation of coda wave attenuation in the Southern Indian Shield and its implications. *Geol. Acta* 10, 309–318.
- Singh, C., Bharathi, V.K.S., Chadha, R.K., 2012b. Lapse time and frequency-dependent attenuation characteristics of Kumaun Himalaya. *J. Asian Earth Sci.* 54, 64–71.
- Singh, D.D., 2005. Rayleigh-wave group-velocity studies beneath the Indian Ocean. *Bull. Seismol. Soc. Am.* 95, 502–511.
- Singh, D.D., 1990. Q-structure beneath the north and central Indian Ocean from the inversion of observed Love and Rayleigh wave attenuation data. *Phys. Earth Planet. Int.* 59, 243–258.
- Singh, D.D., 1988. Crust and upper mantle velocity structure beneath north and central India from the phase and group velocity of Rayleigh and Love waves. *Phys. Earth Planet. Int.* 50, 230–239.
- Singh, S., Herrmann, R.B., 1983. Regionalization of crustal coda Q in the continental United States. *J. Geophys. Res. Solid Earth* 88, 527–538.
- Singh, S.K., Garcia, D., Pacheco, J.F., Valenzuela, R., Bansal, B.K., Dattatrayam, R.S., 2004. Q of the Indian Shield. *Bull. Seismol. Soc. Am.* 94, 1564–1570.
- Souriau, A., 1981. The upper mantle beneath Ninetyeast Ridge and Broken Ridge, Indian Ocean, from surface waves. *Geophys. J. Int.* 67, 359–374.
- Tsuru, T., No, T., Fujie, G., 2017. Geophysical imaging of subsurface structures in volcanic area by seismic attenuation profiling. *Earth, Planets Sp.* 69, 5.
- Vandana, Gupta, S.C., Kumar, A., 2015. Coda wave attenuation characteristics for the Bilaspur region of Himachal Lesser Himalaya. *Nat. Hazards* 78, 1091–1110.
- Vandana, Kumar, A., Gupta, S.C., 2016. Attenuation characteristics of body waves for the Bilaspur region of Himachal Lesser Himalaya. *Pure App. Geophys.* 173, 447–462.
- Vandana, Kumar V., Mishra, O.P., 2019;al, submitted for publication. Seismic Attenuation characteristics of the Northwest Himalaya and its surrounding region and their implications to seismogenesis and seismic hazard. *Bull. Seismol. Soc. Am.* (submitted for publication).
- Venkatesan, S., Gamage, P., 2013. Spectral analysis of seismic waves in the northern Indian Ocean region. *Bull. Seismol. Soc. Am.* 103, 3305–3320.
- Verma, R.K., Mukhopadhyay, M., Bhui, N.C., 1978. Seismicity, gravity and tectonics in the Andaman sea. *J. Phys. Earth* 26, S233–S248.
- Wessel, P., Smith, W.H., 1998. New, improved version of Generic Mapping Tools released. *Eos, Transact. Am. Geophys. Union* 79 (47) 579–579.
- Woodgold, C.R.D., 1994. Coda Q in the Charlevoix, Quebec, Region: lapse-time dependence and spatial and temporal comparisons. *Bull. Seismol. Soc. Am.* 84, 1123–1131.
- Wu, R.S., Aki, K., 1985. Scattering characteristics of elastic waves by an elastic heterogeneity. *Geophysics* 50 (4), 582–595.
- Yang, Y., Forsyth, D.W., Weeraratne, D.S., 2007. Seismic attenuation near the East Pacific Rise and the origin of the low-velocity zone. *Earth Planet. Sci. Lett.* 258, 260–268.
- Yoshimoto, K., Sato, H., Ohtake, M., 1993. Frequency-dependent attenuation of P and S waves in the Kanto area, Japan, based on the coda normalization method. *Geophys. J. Int.* 114, 165–174.
- Yadav, R.K., Kundu, B., Gahalaut, K., Catherine, J., Gahalaut, V.K., Ambikapthy, A., Naidu, M.S., 2013. Coseismic offsets due to the 11 April 2012 Indian Ocean earthquakes (Mw 8.6 and 8.2) derived from GPS measurements. *Geophys. Res. Lett.* 40 (13), 3389–3393.
- Zhao, D., 2015. Multiscale Seismic Tomography. Springer, pp. 304.